

ICES REPORT 12-16

April 2012

Isogeometric Divergence-conforming B-splines for the Unsteady Navier-Stokes Equations

by

John A. Evans and Thomas J.R. Hughes



The Institute for Computational Engineering and Sciences
The University of Texas at Austin
Austin, Texas 78712

Reference: John A. Evans and Thomas J.R. Hughes, Isogeometric Divergence-conforming B-splines for the Unsteady Navier-Stokes Equations, ICES REPORT 12-16, The Institute for Computational Engineering and Sciences, The University of Texas at Austin, April 2012.

Report Documentation Page

Form Approved
OMB No. 0704-0188

Public reporting burden for the collection of information is estimated to average 1 hour per response, including the time for reviewing instructions, searching existing data sources, gathering and maintaining the data needed, and completing and reviewing the collection of information. Send comments regarding this burden estimate or any other aspect of this collection of information, including suggestions for reducing this burden, to Washington Headquarters Services, Directorate for Information Operations and Reports, 1215 Jefferson Davis Highway, Suite 1204, Arlington VA 22202-4302. Respondents should be aware that notwithstanding any other provision of law, no person shall be subject to a penalty for failing to comply with a collection of information if it does not display a currently valid OMB control number.

1. REPORT DATE APR 2012	2. REPORT TYPE	3. DATES COVERED 00-00-2012 to 00-00-2012			
4. TITLE AND SUBTITLE Isogeometric Divergence-conforming B-splines for the Unsteady Navier-Stokes Equations		5a. CONTRACT NUMBER			
		5b. GRANT NUMBER			
		5c. PROGRAM ELEMENT NUMBER			
6. AUTHOR(S)		5d. PROJECT NUMBER			
		5e. TASK NUMBER			
		5f. WORK UNIT NUMBER			
7. PERFORMING ORGANIZATION NAME(S) AND ADDRESS(ES) University of Texas at Austin, Institute for Computational Engineering and Sciences, Austin, TX, 78712		8. PERFORMING ORGANIZATION REPORT NUMBER			
9. SPONSORING/MONITORING AGENCY NAME(S) AND ADDRESS(ES)		10. SPONSOR/MONITOR'S ACRONYM(S)			
		11. SPONSOR/MONITOR'S REPORT NUMBER(S)			
12. DISTRIBUTION/AVAILABILITY STATEMENT Approved for public release; distribution unlimited					
13. SUPPLEMENTARY NOTES					
14. ABSTRACT Divergence-conforming B-splines are developed for application to the incompressible Navier-Stokes equations on geometrically mapped domains. These enable smooth pointwise divergence-free solutions and thus satisfy mass conservation in the strongest possible sense. Semi-discrete methods based on divergence-conforming B-splines are shown to conserve linear and angular momentum and satisfy balance laws for energy vorticity, enstrophy, and helicity. These are geometric structure-preserving quantities and numerical simulations that are sensitive to them are shown to be qualitatively correct and quantitatively accurate. The methods developed are anticipated to open new doors to the practical calculation of complex flows and to studies of their physical behavior.					
15. SUBJECT TERMS					
16. SECURITY CLASSIFICATION OF:			17. LIMITATION OF ABSTRACT	18. NUMBER OF PAGES	19a. NAME OF RESPONSIBLE PERSON
a. REPORT unclassified	b. ABSTRACT unclassified	c. THIS PAGE unclassified	Same as Report (SAR)	48	

Isogeometric Divergence-conforming B-splines for the Unsteady Navier-Stokes Equations

John A. Evans ^{a,*} and Thomas J.R. Hughes ^a

^a *Institute for Computational Engineering and Sciences, The University of Texas at Austin,*

^{*} Corresponding author. *E-mail address:* evans@ices.utexas.edu

Abstract

Divergence-conforming B-splines are developed for application to the incompressible Navier-Stokes equations on geometrically mapped domains. These enable smooth, pointwise divergence-free solutions and thus satisfy mass conservation in the strongest possible sense. Semi-discrete methods based on divergence-conforming B-splines are shown to conserve linear and angular momentum and satisfy balance laws for energy, vorticity, enstrophy, and helicity. These are geometric structure-preserving quantities and numerical simulations that are sensitive to them are shown to be qualitatively correct and quantitatively accurate. The methods developed are anticipated to open new doors to the practical calculation of complex flows and to studies of their physical behavior.

Keywords: Incompressible Navier-Stokes equations, B-splines, Isogeometric analysis, Divergence-conforming discretizations, Structure-preserving discretizations

1 Introduction

The unsteady incompressible Navier-Stokes equations are infused with vast geometric structure, evidenced by a wide array of balance laws for momentum, angular momentum, energy, vorticity, enstrophy, and helicity. These balance laws are considered to be of prime importance in the evolution of laminar and turbulent flow structures [38, 39, 40, 41], and they are even believed to play a role in the regularity of Navier-Stokes solutions [8, 32]. The key to unlocking much of the geometric structure of Navier-Stokes flow is precisely its volume-preserving nature, yet most numerical methods only satisfy the incompressibility constraint in an approximate sense. Consequently, such methods do not obey many fundamental laws of physics. In particular, semi-discretizations which conserve momentum are typically guaranteed to balance energy if and only if the incompressibility constraint is satisfied pointwise. This is especially concerning as energy plays a fundamental role in numerical stability [35].

In this paper, we present new divergence-conforming B-spline semi-discretizations for the unsteady Navier-Stokes problem. These semi-discretizations are motivated by the theory of isogeometric discrete differential forms [12, 13] and extend the steady Navier-Stokes discretizations presented in [23] to unsteady Navier-Stokes flows. As incompressibility is satisfied pointwise, these semi-discretizations replicate the geometric structure of the unsteady Navier-Stokes equations and admit discrete balance laws for momentum, angular momentum, energy, vorticity, enstrophy, and helicity. In this sense, our semi-discretization scheme may be thought of as a structure-preserving or mimetic discretization procedure for the unsteady Navier-Stokes equations. We impose no-penetration boundary conditions strongly and no-slip boundary conditions weakly using Nitsche’s method. This enables our method to handle boundary layers without resorting to stretched meshes [6, 7]. This also allows our discretization procedure to naturally default to a conforming approximation of Euler flow in the limit of vanishing viscosity and to possess both energy and helicity as inviscid invariants. The proposed semi-discretizations are extended to general mapped geometries of scientific and engineering interest using divergence- and integral-preserving transformations for velocity and pressure fields respectively. In addition to all the features mentioned above, a recent paper of Guermond [24] suggests that our semi-discretizations converge to physically relevant weak solutions satisfying a local (in space-time) energy balance. It is not known at this time whether or not such a convergence property holds for spectral semi-discretizations.

The use of B-splines in the numerical analysis of unsteady Navier-Stokes flow has already been conducted with much success. The novelty of the method presented here is simply the use of tensor-product B-splines that are capable of exactly satisfying the incompressibility constraint. In the Direct Numerical Simulation (DNS) community, a common method of choice in simulating wall-bounded flows is the use of Fourier spectral discretizations in periodic directions and B-splines in wall-normal directions [33, 34, 37]. In this setting, B-splines are often preferred over polynomial-based spectral discretizations due to their high resolving power, easy implementation of boundary conditions, and ability to employ stretched grids. Recently, Bazilevs *et al.* studied the turbulence problem in a series of papers using NURBS-based isogeometric analysis in conjunction with a Variational Multiscale (VMS) methodology. In these papers, it was found that the increased continuity of splines led to enhanced numerical results [1, 3, 4, 6, 7]. It is believed that much of this success can be attributed to the spectral-like properties of B-splines. In Figure 1, we have plotted the phase errors associated with one-dimensional k -method NURBS (which in this setting reduce to B-splines of maximal continuity) and C^0 finite element discretizations of the first-order wave equation. Note that the phase error associated with the quadratic NURBS solution is much smaller than that associated with the quadratic finite element solution. Indeed, it can be shown that the phase error for C^{p-1} NURBS solutions scales like $O(h^{2p+2})$ while the phase error for C^0 finite element solutions scales like $O(h^{2p})$ (see Chapter 9 of [15]). Recently, the theory of Kolmogorov n -widths has been utilized to shed more light on the approximation properties of B-splines [20]. In this study, it was revealed that B-splines are much more accurate on a per degree-of-freedom basis than standard finite elements and possess similar approximation properties to that of a spectral

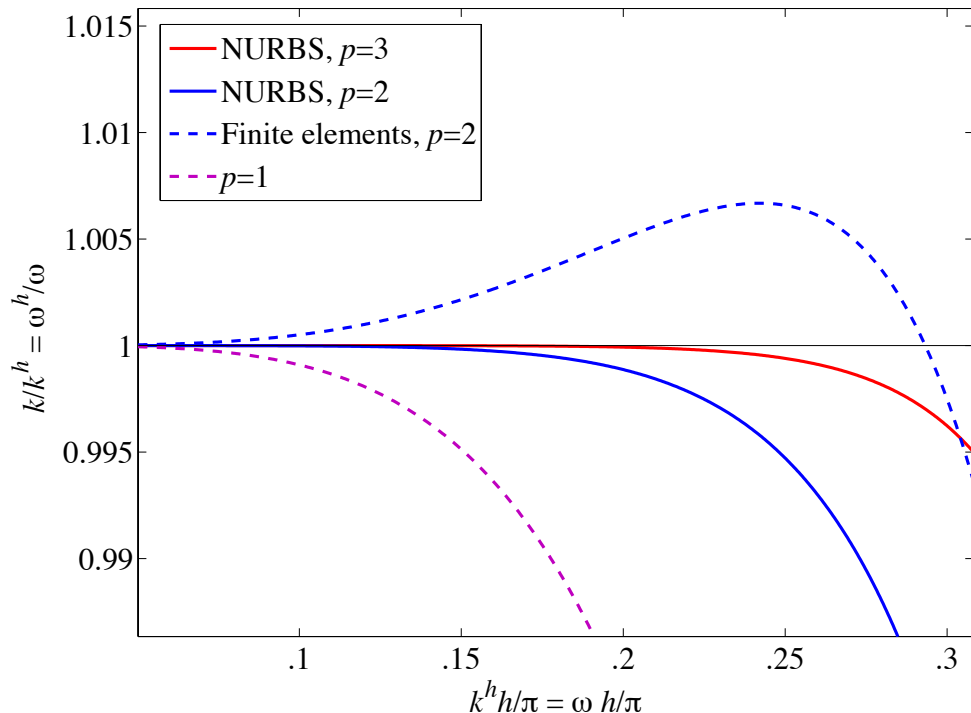


Figure 1: The first-order wave equation. Phase errors versus non-dimensional wave numbers. Comparison of linear and quadratic finite elements, C^1 quadratic NURBS, and C^2 cubic NURBS.

basis. We believe that by combining the spectral-like properties of B-splines with the preservation of the geometric structure of the unsteady Navier-Stokes equations, our semi-discretization procedure may become a useful tool for both engineering analysis and the mathematical study of the unsteady Navier-Stokes equations.

An outline of this paper is as follows. In the following section, we present some basic notation. In Section 3, we recall the unsteady Navier-Stokes problem subject to homogeneous Dirichlet boundary conditions. In Section 4, we briefly review B-splines, the basic building blocks of our new discretization technique, and in Section 5, we define the B-spline spaces which we will utilize to discretize velocity and pressure fields. In Section 6, we present our semi-discrete variational formulation for the steady Navier-Stokes problem, prove well-posedness and a discrete energy inequality, and present an *a priori* error estimate. In Section 7, we derive various balance laws for our semi-discretizations, including balance of linear and angular momentum, energy, vorticity, enstrophy, and helicity. In Section 8, we present numerical results illustrating the advantages of our semi-discretization procedure on three benchmark problems: two-dimensional Taylor-Green vortex flow, alternating cylindrical Couette flow, and three-dimensional Taylor-Green vortex flow. Each of these problems is sensitive to preservation of conserved quantities and the growth and decay of functionals associated with geometrical structure of the flow. In Section 9, we draw conclusions. Before proceeding, it should be mentioned that we do not consider any artificial

diffusion mechanisms or subgrid turbulence models in this paper. As such, the semi-discretizations presented here should only be utilized if the flow field is sufficiently resolved by the spatial mesh. That being said, standard Large Eddy Simulation models can be utilized in conjunction with the proposed semi-discretizations to capture fine-scale turbulent effects on coarse meshes.

2 Notation

We begin this paper with some basic notation. For d a positive integer representing dimension, let $D \subset \mathbb{R}^d$ denote an arbitrary bounded Lipschitz domain with boundary ∂D . As usual, let $L^2(D)$ denote the space of square integrable functions on D and define $\mathbf{L}^2(D) = (L^2(D))^d$. We denote $L_0^2(D) \subset L^2(D)$ as the space of square-integrable functions with zero average on D . We will also utilize the more general Lebesgue spaces $L^p(D)$ where $1 \leq p \leq \infty$. Let $H^k(D)$ denote the space of functions in $L^2(D)$ whose k^{th} -order derivatives belong to $L^2(D)$ and define $\mathbf{H}^k(D) = (H^k(D))^d$. We identify with $H^k(D)$ the standard Sobolev norm

$$\|v\|_{H^k(D)} = \left(\sum_{|\boldsymbol{\alpha}| < k} \|D^{\boldsymbol{\alpha}} v\|_{L^2(D)}^2 \right)^{1/2}$$

where $\boldsymbol{\alpha} = (\alpha_1, \alpha_2, \dots, \alpha_d)$ is a multi-index of non-negative integers, $|\boldsymbol{\alpha}| = \alpha_1 + \alpha_2 + \dots + \alpha_d$, and

$$D^{\boldsymbol{\alpha}} = \frac{\partial^{|\boldsymbol{\alpha}|}}{\partial x_1^{\alpha_1} \partial x_2^{\alpha_2} \dots \partial x_d^{\alpha_d}}.$$

We denote the Sobolev semi-norms as $|\cdot|_{H^k(D)}$, and we adopt the convention $H^0(D) = L^2(D)$. Throughout, Sobolev spaces of fractional order are defined using function space interpolation (see, e.g., Chapter 1 of [48]). We define $H_0^1(D) \subset H^1(D)$ to be the subspace of functions with homogeneous boundary conditions and define $\mathbf{H}_0^1(D)$ to be the vectorial counterpart of $H_0^1(D)$. We define $\mathbf{H}(\text{div}; D)$ to be the Sobolev space of all functions in $\mathbf{L}^2(D)$ whose divergence belongs to $L^2(D)$. This space is equipped with the norm

$$\|\mathbf{v}\|_{\mathbf{H}(\text{div}; D)} = \left(\|\mathbf{v}\|_{\mathbf{L}^2(D)}^2 + \|\text{div } \mathbf{v}\|_{L^2(D)}^2 \right)^{1/2}.$$

We also define

$$\mathbf{H}_0(\text{div}; D) = \{\mathbf{v} \in \mathbf{H}(\text{div}; D) : \mathbf{v} \cdot \mathbf{n} = 0 \text{ on } \partial D\}$$

where \mathbf{n} denotes the outward pointing unit normal. Finally, for X a real Banach space and S a positive real number, we define $L^q(0, S; X)$ as the space consisting of all strongly measurable functions $\phi : (0, S) \rightarrow X$ with

$$\|\phi\|_{L^q(0, S; X)} := \left(\int_0^S \|\phi(t)\|_X^q dt \right)^{1/q} < \infty \quad (1)$$

for $1 \leq q < \infty$ and

$$\|\phi\|_{L^\infty(0,S;X)} := \text{ess sup}_{0 < t < S} \|\phi(t)\|_X < \infty, \quad (2)$$

and $C^0([0, S]; X)$ as the space of all continuous functions $\phi : [0, S] \rightarrow X$.

3 The Unsteady Navier-Stokes Problem

In this section, we recall the unsteady Navier-Stokes problem subject to homogeneous Dirichlet boundary conditions. For d a positive integer, let Ω denote a Lipschitz bounded open set of \mathbb{R}^d . Throughout this paper, d will be either 2 or 3. The problem of interest is as follows.

$$(S) \left\{ \begin{array}{l} \text{Given } \nu \in \mathbb{R}^+, \mathbf{f} : \Omega \times (0, \infty) \rightarrow \mathbb{R}^d, \text{ and } \mathbf{u}_0 : \Omega \rightarrow \mathbb{R}^d, \text{ find } \mathbf{u} : \\ \bar{\Omega} \times [0, \infty) \rightarrow \mathbb{R}^d \text{ and } p : \Omega \times (0, \infty) \rightarrow \mathbb{R} \text{ such that} \\ \\ \frac{\partial \mathbf{u}}{\partial t} + \nabla \cdot (\mathbf{u} \otimes \mathbf{u}) + \mathbf{grad} p - \nabla \cdot (2\nu \nabla^s \mathbf{u}) = \mathbf{f} \quad (3) \\ \text{div } \mathbf{u} = 0 \quad (4) \\ \\ \text{in } \Omega \times (0, \infty) \text{ and} \\ \\ \mathbf{u} = \mathbf{0} \quad \text{on } \partial\Omega \times (0, \infty) \quad (5) \\ \mathbf{u}(\cdot, 0) = \mathbf{u}_0(\cdot) \quad \text{in } \Omega. \quad (6) \end{array} \right.$$

Above, \mathbf{u} denotes the flow velocity of a fluid moving through the domain Ω , p denotes the pressure acting on the fluid divided by the fluid density, ν denotes the kinematic viscosity of the fluid, \mathbf{f} denotes a body force acting on the fluid divided by the density, and $\nabla^s \mathbf{u}$ denotes the symmetrized gradient of the velocity field defined by

$$\nabla^s \mathbf{u} = \frac{1}{2} \left(\nabla \mathbf{u} + (\nabla \mathbf{u})^T \right).$$

An appropriate definition of weak solution is not entirely obvious in the context of unsteady Navier-Stokes flows, especially for domains in \mathbb{R}^3 . The most basic type of weak solution is a so-called Leray-Hopf solution. Given a fixed end-time $T > 0$, let us assume that $\mathbf{f} \in L^\infty(0, T; \mathbf{L}^2(\Omega))$ and

$$\mathbf{u}_0 \in \{ \mathbf{u} \in \mathbf{H}_0(\text{div}; \Omega) : \text{div } \mathbf{u} = 0 \}.$$

A Leray-Hopf solution over the time interval $(0, T)$ is then defined as a vector function $\mathbf{u} \in L^\infty(0, T; \mathbf{L}^2(\Omega)) \cap L^2(0, T; \mathbf{H}_0^1(\Omega))$ satisfying $\mathbf{u}(\cdot, 0) = \mathbf{u}_0$, $\text{div } \mathbf{u} = 0$ in the sense of distributions, the energy inequality

$$\|\mathbf{u}(t)\|_{\mathbf{L}^2(\Omega)}^2 + \int_0^t 4\nu \|\nabla^s \mathbf{u}(s)\|_{(L^2(\Omega))^{d \times d}}^2 ds \leq \|\mathbf{u}(0)\|_{\mathbf{L}^2(\Omega)}^2 + \int_0^t 2(\mathbf{f}(s), \mathbf{u}(s))_{\mathbf{L}^2(\Omega)} ds \quad (7)$$

for almost every $t \in (0, T)$, and

$$\int_0^T \int_{\Omega} (\mathbf{u} \cdot \partial_t \mathbf{v} + (\mathbf{u} \otimes \mathbf{u}) : \nabla \mathbf{v} + \mathbf{u} \cdot \nabla \cdot (2\nu \nabla^s \mathbf{v}) + \mathbf{f} \cdot \mathbf{v}) \, dx dt + \int_{\Omega} \mathbf{u}_0 \cdot \mathbf{v} \, dx = 0 \quad (8)$$

for all smooth test functions $\mathbf{v} \in (C_0^\infty((0, T) \times \Omega))^d$ such that $\operatorname{div} \mathbf{v} = 0$. In 1934, Leray obtained the first three-dimensional existence results for the Navier-Stokes equations by carefully constructing a Leray-Hopf weak solution for the Navier-Stokes problem posed on all of \mathbb{R}^3 [36], and seventeen years later, Hopf extended this existence result to the Dirichlet problem by constructing a Leray-Hopf solution as the limit of a sequence of Galerkin approximations [30]. While the question of existence was answered many decades ago for Leray-Hopf solutions, the question of uniqueness remains unanswered for domains in \mathbb{R}^3 . This is primarily due to an intimate relationship between uniqueness and regularity [18]. *A priori* estimates have not yet been able to preclude the occurrence of so-called vorticity bursts reaching scales smaller than the Kolmogorov scale due to the presence of enstrophy production. In his seminal 1977 paper, Scheffer introduced a systematic means of addressing the regularity question by studying the Hausdorff measure of the singular set of weak solutions [45]. If one can prove the measure of this set is zero, one will then have answered the Navier-Stokes smoothness question in the affirmative. To systematically study the Hausdorff measure, Scheffer introduced so-called suitable weak solutions which satisfy a local space-time energy balance. Specifically, suitable weak solutions satisfy the inequality

$$\partial_t \left(\frac{1}{2} |\mathbf{u}|^2 \right) + \nabla \cdot \left(\left(\frac{1}{2} |\mathbf{u}|^2 + p \right) \mathbf{u} \right) - \nu \nabla^2 \left(\frac{1}{2} |\mathbf{u}|^2 \right) + \nu |\nabla \mathbf{u}|^2 - \mathbf{f} \cdot \mathbf{u} \leq 0 \quad (9)$$

in a distributional sense. Such a local balance can be interpreted as an “entropy condition” for incompressible flows. Suitable weak solutions are known to always exist, and they may be obtained via a regularization of the Navier-Stokes equations and passing to the limit. With the notion of a suitable weak solution, Scheffer was able to derive a bound from above of some Hausdorff measure of the singular set. This bound was then improved upon in the famous 1982 paper of Caffarelli, Kohn, and Nirenberg where it is proven that the one-dimensional Hausdorff measure of the set of singularities for a suitable weak solution is zero [14]. That is, if singularities exist, they cannot lie along a line in space-time. This is widely considered to be the best general result in the direction of the Navier-Stokes Millenium Prize Problem.

All of the above machinery is not necessary in the derivation of a semi-discrete variational formulation. As we will show later in this paper, we are able to obtain a well-posed semi-discrete problem via a simple Galerkin methodology. That being said, a recent paper of Guermond suggests that our semi-discrete formulation converges to a suitable weak solution [24]. It should be noted that it is not known whether or not such a convergence property holds for spectral discretizations which are the standard in direct numerical simulation of turbulent flows. It is possible that spectral discretizations may not converge to suitable weak solutions as they do not induce enough numerical diffusion to counteract the Gibbs-Wilbraham phenomenon, preventing a local energy balance from holding in the limit [25].

4 B-splines and Geometrical Mappings

In this section, we briefly introduce B-splines, the primary ingredient in our discretization technique for the unsteady Navier-Stokes equations. We also introduce mappings which will allow us to extend our discretization technique to general geometries of engineering interest. For an overview of B-splines, their properties, and robust algorithms for evaluating their values and derivatives, see de Boor [17] and Schumaker [46]. For the application of B-splines to finite element analysis, see Höllig [29] and Cottrell, Hughes, and Bazilevs [15].

4.1 Univariate B-splines

For two positive integers k and n , representing degree and dimensionality respectively, let us introduce the ordered knot vector

$$\Xi := \{0 = \xi_1, \xi_2, \dots, \xi_{n+k+1} = 1\} \quad (10)$$

where

$$\xi_1 \leq \xi_2 \leq \dots \leq \xi_{n+k+1}.$$

Given Ξ and k , univariate B-spline basis functions are constructed recursively starting with piecewise constants ($k = 0$):

$$B_i^0(\xi) = \begin{cases} 1 & \text{if } \xi_i \leq \xi < \xi_{i+1} \\ 0 & \text{otherwise.} \end{cases} \quad (11)$$

For $k = 1, 2, 3, \dots$, they are defined by the Cox-de Boor recursion formula:

$$B_i^k(\xi) = \frac{\xi - \xi_i}{\xi_{i+k} - \xi_i} B_i^{k-1}(\xi) + \frac{\xi_{i+k+1} - \xi}{\xi_{i+k+1} - \xi_{i+1}} B_{i+1}^{k-1}(\xi). \quad (12)$$

When $\xi_{i+k} - \xi_i = 0$, $\frac{\xi - \xi_i}{\xi_{i+k} - \xi_i}$ is taken to be zero, and similarly, when $\xi_{i+k+1} - \xi_{i+1} = 0$, $\frac{\xi_{i+k+1} - \xi}{\xi_{i+k+1} - \xi_{i+1}}$ is taken to be zero. B-spline basis functions are piecewise polynomials of degree k , form a partition of unity, have local support, and are non-negative. We refer to linear combinations of B-spline basis functions as B-splines or simply splines.

Let us now introduce the vector $\zeta = \{\zeta_1, \dots, \zeta_m\}$ of knots without repetitions and a corresponding vector $\{r_1, \dots, r_m\}$ of knot multiplicities. That is, r_i is defined to be the multiplicity of the knot ζ_i in Ξ . We assume that $r_i \leq k + 1$. Let us further assume throughout that $r_1 = r_m = k + 1$, *i.e.*, that Ξ is an open knot vector. This allows us to easily prescribe Dirichlet boundary conditions. At the point ζ_i , B-spline basis functions have $\alpha_j := k - r_j$ continuous derivatives. We define the regularity vector α by $\alpha := \{\alpha_1, \dots, \alpha_m\}$. By construction, $\alpha_1 = \alpha_m = -1$. In what follows, we utilize the notation

$$|\alpha| = \min\{\alpha_i : 2 \leq i \leq m - 1\} \quad (13)$$

and $\alpha - 1 := \{-1, \alpha_2 - 1, \dots, \alpha_{m-1} - 1, -1\}$ when $\alpha_i \geq 0$ for $2 \leq i \leq m - 1$.

We denote the space of B-splines spanned by the basis functions B_i^k as

$$S_{\alpha}^k := \text{span} \{B_i^k\}_{i=1}^n. \quad (14)$$

When $k \geq 1$ and $\alpha_i \geq 0$ for $2 \leq i \leq m-1$, the derivatives of functions in S_{α}^k are splines as well. In fact, we have the stronger relationship

$$\left\{ \frac{d}{dx} v : v \in S_{\alpha}^k \right\} \equiv S_{\alpha-1}^{k-1}. \quad (15)$$

One of the most important properties of univariate B-splines is refinement and, perhaps more importantly, nestedness of refinement. Knot insertion and degree elevation algorithms are described in detail in Chapter 2 of [15].

4.2 Multivariate B-splines

The definition of multivariate B-splines follows easily through a tensor-product construction. For d again a positive integer, let us consider the unit cube $\bar{\Omega} = (0, 1)^d \subset \mathbb{R}^d$, which we will henceforth refer to as the parametric domain. Mimicking the one-dimensional case, given integers k_l and n_l for $l = 1, \dots, d$, let us introduce open knot vectors $\Xi_l = \{\xi_{1,l}, \dots, \xi_{n_l+k_l+1,l}\}$ and the associated vectors $\zeta_l = \{\zeta_{1,l}, \dots, \zeta_{m_l,l}\}$, $\{r_{1,l}, \dots, r_{m_l,l}\}$, and $\alpha_l = \{\alpha_{1,l}, \dots, \alpha_{m_l,l}\}$. There is a parametric Cartesian mesh \mathcal{M}_h associated with these knot vectors partitioning the parametric domain into rectangular parallelepipeds. Visually,

$$\mathcal{M}_h = \{Q = \otimes_{l=1, \dots, d} (\zeta_{i_l,l}, \zeta_{i_l+1,l}), 1 \leq i_l \leq m_l - 1\}. \quad (16)$$

For each element $Q \in \mathcal{M}_h$ we associate a parametric mesh size $h_Q = \text{diam}(Q)$. We also define a shape regularity constant λ which satisfies the inequality

$$\lambda^{-1} \leq \frac{h_{Q,\min}}{h_Q} \leq \lambda, \quad \forall Q \in \mathcal{M}_h, \quad (17)$$

where $h_{Q,\min}$ denotes the length of the smallest edge of Q . A sequence of parametric meshes that satisfy the above inequality for an identical shape regularity constant is said to be quasi-uniform.

We associate with each knot vector Ξ_l ($l = 1, \dots, d$) univariate B-spline basis functions $B_{i_l,l}^{k_l}$ of degree k_l for $i_l = 1, \dots, n_l$. On the mesh \mathcal{M}_h , we define the tensor-product B-spline basis functions as

$$B_{i_1, \dots, i_d}^{k_1, \dots, k_d} := B_{i_1,1}^{k_1} \otimes \dots \otimes B_{i_d,d}^{k_d}, \quad i_1 = 1, \dots, n_1, \dots, i_d = 1, \dots, n_d. \quad (18)$$

We then accordingly define the tensor-product B-spline space as

$$S_{\alpha_1, \dots, \alpha_d}^{k_1, \dots, k_d} \equiv S_{\alpha_1, \dots, \alpha_d}^{k_1, \dots, k_d}(\mathcal{M}_h) := \text{span} \left\{ B_{i_1, \dots, i_d}^{k_1, \dots, k_d} \right\}_{i_1=1, \dots, i_d=1}^{n_1, \dots, n_d}. \quad (19)$$

Like their univariate counterparts, multivariate B-spline basis functions are piecewise polynomial, form a partition of unity, have local support, and are non-negative. Defining the regularity constant

$$\alpha := \min_{l=1,\dots,d} \min_{2 \leq i_l \leq m_l - 1} \{\alpha_{i_l, l}\} \quad (20)$$

we see that our B-splines are C^α -continuous throughout the domain $\widehat{\Omega}$. Refinement of multivariate B-spline bases is obtained by applying knot insertion and degree elevation in tensor-product fashion. In the remainder of this paper, we consider a family of nested meshes $\{\mathcal{M}_h\}_{h \leq h_0}$ and associated B-spline spaces $\{S_{\alpha_1, \dots, \alpha_d}^{k_1, \dots, k_d}(\mathcal{M}_h)\}_{h \leq h_0}$ that have been obtained by successive applications of knot refinement. Furthermore, we assume throughout that the mesh family $\{\mathcal{M}_h\}_{h \leq h_0}$ is quasi-uniform.

Note that each element $Q = \otimes_{l=1, \dots, d} (\zeta_{i_l, l}, \zeta_{i_l+1, l})$ has the equivalent representation $Q = \otimes_{l=1, \dots, d} (\xi_{j_l, l}, \xi_{j_l+1, l})$ for some index j_l . With this in mind, we associate with each element a support extension \tilde{Q} , defined as

$$\tilde{Q} := \otimes_{l=1, \dots, d} (\xi_{j_l - k_l, l}, \xi_{j_l + k_l + 1, l}). \quad (21)$$

The support extension is the interior of the set formed by the union of the supports of all B-spline basis functions whose support intersects Q . Note that each element belongs to the support extension of at most $\prod_{l=1, \dots, d} (2k_l + 1)$ elements.

4.3 Piecewise Smooth Functions, Geometrical Mappings, and Physical Mesh Entities

On the parametric mesh \mathcal{M}_h , we define the space of piecewise smooth functions with interelement regularity given by the vectors $\alpha_1, \dots, \alpha_d$ as

$$C_{\alpha_1, \dots, \alpha_d}^\infty = C_{\alpha_1, \dots, \alpha_d}^\infty(\mathcal{M}_h). \quad (22)$$

Precisely, a function in $C_{\alpha_1, \dots, \alpha_d}^\infty$ is a function whose restriction to an element $Q \in \mathcal{M}_h$ admits a C^∞ extension in the closure of that element and which has $\alpha_{i_l, l}$ continuous derivatives with respect to the l th coordinate along the internal mesh faces $\{(x_1, \dots, x_d) : x_l = \zeta_{i_l, l}, \zeta_{j_{l'}, l'} < x_{l'} < \zeta_{j_{l'}+1, l'}, l' \neq l\}$ for all $i_l = 2, \dots, m_l - 1$ and $j_{l'} = 1, \dots, m_{l'} - 1$. Note immediately that any function lying in the B-spline space $S_{\alpha_1, \dots, \alpha_d}^{k_1, \dots, k_d}$ also lies in $C_{\alpha_1, \dots, \alpha_d}^\infty$.

Unless specified otherwise, we assume throughout the rest of the paper that the physical domain $\Omega \subset \mathbb{R}^d$ can be exactly parametrized by a geometrical mapping $\mathbf{F} : \widehat{\Omega} \rightarrow \Omega$ belonging to $(C_{\alpha_1, \dots, \alpha_d}^\infty)^d$ with piecewise smooth inverse. We further assume that the physical domain Ω is simply connected with connected boundary $\partial\Omega$ and the geometrical mapping is independent of the mesh family index h . The geometrical mapping \mathbf{F} naturally induces a mesh

$$\mathcal{K}_h = \{K : K = \mathbf{F}(Q), Q \in \mathcal{M}_h\} \quad (23)$$

on the physical domain Ω . We define for each element $K \in \mathcal{K}_h$ a physical mesh size

$$h_K = \|D\mathbf{F}\|_{L^\infty(Q)} h_Q \quad (24)$$

where Q is the pre-image of K , and we also define the support extension $\tilde{K} = \mathbf{F}(\tilde{Q})$. We define for a given mesh the global mesh size

$$h = \max \{h_K, K \in \mathcal{K}_h\}.$$

Note that as the parametric mesh family $\{\mathcal{M}_h\}_{h \leq h_0}$ is quasi-uniform and the geometrical mapping \mathbf{F} is independent of the mesh family index h , the physical mesh family $\{\mathcal{K}_h\}_{h \leq h_0}$ is also quasi-uniform. We refer to the physical domain Ω and its pre-image $\hat{\Omega}$ interchangeably as the patch. It should be noted that, in general, the domain Ω cannot be represented using just a single patch. Instead, multiple patches must be employed. For the sake of brevity, the multi-patch setting will not be covered in this paper. The interested reader is referred to [19, 22, 23]

We define on the parametric mesh a set of mesh faces $\hat{\mathcal{F}}_h = \{\hat{F}\}$ where \hat{F} is a face of one or more elements in \mathcal{M}_h . We define the physical set of mesh faces as

$$\mathcal{F}_h = \{F = \mathbf{F}(\hat{F}) : \hat{F} \in \hat{\mathcal{F}}_h\}$$

and we define the boundary mesh to be

$$\Gamma_h = \{F \in \mathcal{F}_h : F \subset \partial\Omega\}.$$

By construction,

$$\partial\Omega = \cup_{F \in \Gamma_h} \bar{F}.$$

Note that for each face $F \in \Gamma_h$ there is a unique $K \in \mathcal{K}_h$ such that F is a “face” of K (in the sense that F is the image of a face of Q , the pre-image of K). We hence define for such a face the mesh size

$$h_F := h_K.$$

One may also define h_F to be the wall-normal mesh-size as is done in [6].

5 Discretization of Velocity and Pressure Fields

In this section, we define the B-spline spaces which we will utilize to discretize the velocity and pressure fields appearing in the unsteady Navier-Stokes problem. These spaces are motivated by the recent theory of isogeometric discrete differential forms [12, 13] and may be interpreted as smooth generalizations of Raviart-Thomas elements [44]. For a more in-depth discussion of the discrete velocity and pressure spaces used in this paper, see Section 5 of [22].

5.1 Discrete Spaces on the Parametric Domain

Using the notation of the previous section and assuming that

$$\alpha := \min\{|\boldsymbol{\alpha}_l| : l = 1, \dots, d\} \geq 1,$$

we define the following two spaces:

$$\widehat{\mathcal{V}}_h := \begin{cases} S_{\alpha_1, \alpha_2-1}^{k_1, k_2-1} \times S_{\alpha_1-1, \alpha_2}^{k_1-1, k_2} & \text{if } d = 2, \\ S_{\alpha_1, \alpha_2-1, \alpha_3-1}^{k_1, k_2-1, k_3-1} \times S_{\alpha_1-1, \alpha_2, \alpha_3-1}^{k_1-1, k_2, k_3-1} \times S_{\alpha_1-1, \alpha_2-1, \alpha_3}^{k_1-1, k_2-1, k_3} & \text{if } d = 3, \end{cases}$$

$$\widehat{\mathcal{Q}}_h := \begin{cases} S_{\alpha_1-1, \alpha_2-1}^{k_1-1, k_2-1} & \text{if } d = 2, \\ S_{\alpha_1-1, \alpha_2-1, \alpha_3-1}^{k_1-1, k_2-1, k_3-1} & \text{if } d = 3. \end{cases}$$

The spaces $\widehat{\mathcal{V}}_h$ and $\widehat{\mathcal{Q}}_h$ are precisely the spaces of discrete two-forms and three-forms that were introduced in [12], and they were first applied to the discretization of Stokes flow in [11]. The space $\widehat{\mathcal{V}}_h$ comprises our set of discrete velocity fields while $\widehat{\mathcal{Q}}_h$ comprises our set of discrete pressure fields. Note that as $\alpha \geq 1$, our discrete velocity fields are \mathbf{H}^1 -conforming. If we allow $\alpha = 0$, our spaces collapse to standard Raviart-Thomas mixed finite elements [44]. In order to deal with no-penetration boundary conditions, we make use of the following constrained discrete spaces:

$$\widehat{\mathcal{V}}_{0,h} := \left\{ \widehat{\mathbf{v}}_h \in \widehat{\mathcal{V}}_h : \widehat{\mathbf{v}}_h \cdot \widehat{\mathbf{n}} = 0 \text{ on } \partial\widehat{\Omega} \right\},$$

$$\widehat{\mathcal{Q}}_{0,h} := \left\{ \widehat{q}_h \in \widehat{\mathcal{Q}}_h : \int_{\widehat{\Omega}} \widehat{q}_h d\widehat{\mathbf{x}} = 0 \right\}.$$

Above, $\widehat{\mathbf{n}}$ denotes the outward-facing normal to $\partial\widehat{\Omega}$. As specified in the introduction, we choose to enforce no-slip boundary conditions weakly using Nitsche's method [42]. Due to the special relationship given by (15), the spaces $\widehat{\mathcal{V}}_{0,h}$ and $\widehat{\mathcal{Q}}_{0,h}$ along with the parametric divergence operator form the bounded discrete cochain complex

$$\widehat{\mathcal{V}}_{0,h} \xrightarrow{\widehat{\text{div}}} \widehat{\mathcal{Q}}_{0,h}$$

where $\widehat{\text{div}}$ is the divergence operator on the unit cube $\widehat{\Omega}$.

5.2 Discrete Spaces on the Physical Domain

To define our discrete velocity and pressure spaces on the physical domain, we introduce the following pullback operators:

$$\iota_u(\mathbf{v}) := \det(D\mathbf{F}) (D\mathbf{F})^{-1} (\mathbf{v} \circ \mathbf{F}), \quad \mathbf{v} \in \mathbf{H}_0(\text{div}; \Omega) \quad (25)$$

$$\iota_p(q) := \det(D\mathbf{F}) (q \circ \mathbf{F}), \quad q \in L_0^2(\Omega) \quad (26)$$

where $D\mathbf{F}$ is the Jacobian matrix of the parametric mapping \mathbf{F} . With these operators defined, we have the following commuting diagram:

$$\begin{array}{ccc} \mathbf{H}_0(\widehat{\text{div}}; \widehat{\Omega}) & \xrightarrow{\widehat{\text{div}}} & L_0^2(\widehat{\Omega}) \\ \iota_u \uparrow & & \iota_p \uparrow \\ \mathbf{H}_0(\text{div}; \Omega) & \xrightarrow{\text{div}} & L_0^2(\Omega). \end{array} \quad (27)$$

This motivates the use of the following discrete velocity and pressure spaces in the physical domain:

$$\begin{aligned}\mathcal{V}_{0,h} &:= \left\{ \mathbf{v} \in \mathbf{H}_0(\text{div}; \Omega) : \iota_u(\mathbf{v}) \in \widehat{\mathcal{V}}_{0,h} \right\}, \\ \mathcal{Q}_{0,h} &:= \left\{ q \in L_0^2(\Omega) : \iota_p(q) \in \widehat{\mathcal{Q}}_{0,h} \right\}.\end{aligned}$$

In [12], it was shown that there exist projection operators $\Pi_{\mathcal{V}_h}^0 : \mathbf{H}_0(\text{div}; \Omega) \rightarrow \mathcal{V}_{0,h}$ and $\Pi_{\mathcal{Q}_h}^0 : L^2(\Omega) \rightarrow \mathcal{Q}_{0,h}$ such that the following proposition holds.

Proposition 5.1. *The following diagram commutes:*

$$\begin{array}{ccc} \mathbf{H}_0(\text{div}; \Omega) & \xrightarrow{\text{div}} & L_0^2(\Omega) \\ \Pi_{\mathcal{V}_h}^0 \downarrow & & \Pi_{\mathcal{Q}_h}^0 \downarrow \\ \mathcal{V}_{0,h} & \xrightarrow{\text{div}} & \mathcal{Q}_{0,h}. \end{array} \quad (28)$$

Furthermore, there exists a positive constant C_u independent of h such that

$$\|\Pi_{\mathcal{V}_h}^0 \mathbf{v}\|_{\mathbf{H}^1(\Omega)} \leq C_u \|\mathbf{v}\|_{\mathbf{H}^1(\Omega)}, \quad \forall \mathbf{v} \in \mathbf{H}_0(\text{div}; \Omega) \cap \mathbf{H}^1(\Omega). \quad (29)$$

We immediately have an inf-sup condition for our discrete velocity/pressure pair as a consequence of the above proposition. A complete proof of the inf-sup condition may be found in [22].

Proposition 5.2. *There exists a positive constant $\mathring{\beta}$ independent of h such that:*

$$\inf_{\substack{q_h \in \mathcal{Q}_{0,h} \\ q_h \neq 0}} \sup_{\mathbf{v}_h \in \mathcal{V}_{0,h}} \frac{(\text{div} \mathbf{v}_h, q_h)_{L^2(\Omega)}}{\|\mathbf{v}_h\|_{\mathbf{H}^1(\Omega)} \|q_h\|_{L^2(\Omega)}} \geq \mathring{\beta}. \quad (30)$$

We also have the following result.

Proposition 5.3. *If $\mathbf{v}_h \in \mathcal{V}_{0,h}$ satisfies*

$$(\text{div} \mathbf{v}_h, q_h)_{L^2(\Omega)} = 0, \quad \forall q_h \in \mathcal{Q}_{0,h}, \quad (31)$$

then $\text{div} \mathbf{v}_h \equiv 0$.

Proof. The proof holds trivially as div maps $\mathcal{V}_{0,h}$ onto $\mathcal{Q}_{0,h}$. □

Hence, by choosing $\mathcal{V}_{0,h}$ and $\mathcal{Q}_{0,h}$ as discrete velocity and pressure spaces, we arrive at an inf-sup stable discretization that automatically returns velocity fields that are pointwise divergence-free.

5.3 Approximation Results and Trace Inequalities

Let us define

$$k' = \min_{l=1,\dots,d} |k_l - 1|. \quad (32)$$

Note that the discrete velocity and pressure spaces $\mathcal{V}_{0,h}$ and $\mathcal{Q}_{0,h}$ consist of mapped piecewise polynomials which are complete up to degree k' . The following result details the local approximation properties of our discrete spaces. Its proof may be found in [12].

Proposition 5.4. *Let $K \in \mathcal{K}_h$ and \tilde{K} denote the support extension of K . For $0 \leq j \leq s \leq k' + 1$, we have*

$$|\mathbf{v} - \Pi_{\mathcal{V}_h}^0 \mathbf{v}|_{\mathbf{H}^j(K)} \leq Ch_K^{s-j} \|\mathbf{v}\|_{\mathbf{H}^s(\tilde{K})}, \quad \forall \mathbf{v} \in \mathbf{H}^s(\tilde{K}) \cap \mathbf{H}_0(\text{div}; \Omega) \quad (33)$$

$$|q - \Pi_{\mathcal{Q}_h}^0 q|_{H^j(K)} \leq Ch_K^{s-j} \|q\|_{H^s(\tilde{K})}, \quad \forall q \in H^s(\tilde{K}) \cap L_0^2(\Omega) \quad (34)$$

where C denotes a positive constant, possibly different at each appearance, independent of h .

Hence, our discrete spaces deliver optimal rates of convergence from an approximation point of view. We will also need the following trace estimate in what follows. Its proof can be found in [19].

Proposition 5.5. *Let $K \in \mathcal{K}_h$. Then we have*

$$\|(\nabla^s \mathbf{v}_h) \mathbf{n}\|_{(L^2(\partial K))^d} \leq C_{\text{trace}} h_K^{-1} \|\mathbf{v}_h\|_{\mathbf{H}^1(K)}, \quad \forall \mathbf{v}_h \in \mathcal{V}_{0,h} \quad (35)$$

where C_{trace} denotes a positive constant independent of h .

In [21], it was shown that Proposition 5.5 holds for B-splines and parametric finite elements with $C_{\text{trace}} \sim (k')^2$. However, our numerical experience has indicated that a corresponding global trace inequality holds with $C_{\text{trace}} \sim k'$ if B-splines of maximal continuity are utilized.

6 The Semi-Discrete Problem

In this section, we approximate the unsteady Navier-Stokes problem using the discrete velocity and pressure spaces introduced in the previous section. We prove the resulting semi-discretization scheme is well-posed and satisfies a discrete energy balance law, and we briefly discuss *a priori* error estimates.

6.1 Semi-Discrete Variational Formulation

We begin this section by presenting a semi-discrete variational formulation for the unsteady Navier-Stokes equations subject to homogeneous Dirichlet boundary conditions. Since members of $\mathcal{V}_{0,h}$ do not satisfy homogeneous tangential Dirichlet boundary conditions, we employ Nitsche's method to weakly enforce no-slip boundary conditions. To this effect, we define the following bilinear form for $C_{\text{pen}} \geq 1$ a chosen

positive penalty constant independent of mesh size:

$$k_h(\mathbf{w}, \mathbf{v}) = k(\mathbf{w}, \mathbf{v}) - \sum_{F \in \Gamma_h} \int_F 2\nu \left(((\nabla^s \mathbf{v}) \mathbf{n}) \cdot \mathbf{w} + ((\nabla^s \mathbf{w}) \mathbf{n}) \cdot \mathbf{v} - \frac{C_{pen}}{h_F} \mathbf{w} \cdot \mathbf{v} \right) ds \quad (36)$$

where

$$k(\mathbf{w}, \mathbf{v}) = (2\nu \nabla^s \mathbf{w}, \nabla^s \mathbf{v})_{(L^2(\Omega))^{d \times d}}, \quad \forall \mathbf{w}, \mathbf{v} \in \mathbf{H}^1(\Omega). \quad (37)$$

Let us also define our discrete space-time velocity space as

$$\mathcal{V}_T^h := \{ \mathbf{v}_h \in C^0((0, T); \mathcal{V}_{0,h}) : \partial_t \mathbf{v}_h \in L^2((0, T); \mathcal{V}_{0,h}) \} \quad (38)$$

and our discrete space-time pressure space as

$$\mathcal{Q}_T^h := L^2((0, T); \mathcal{Q}_{0,h}). \quad (39)$$

It remains to specify our discrete initial condition. In what follows, we choose $\mathbf{u}_{0,h} = \Pi_{\mathcal{V}_h}^0 \mathbf{u}_0$. Note that, by construction, $\text{div} \mathbf{u}_{0,h} = 0$. We can alternatively specify our initial condition through \mathbf{H}^1 -projection into the B-spline space of divergence-free fields. This amounts to solving a steady Stokes problem as a pre-processing step. Employing the terminology defined above, our semi-discrete formulation reads as follows.

$$(G) \left\{ \begin{array}{l} \text{Find } \mathbf{u}_h \in \mathcal{V}_T^h \text{ and } p_h \in \mathcal{Q}_T^h \text{ such that } \mathbf{u}_h(0) = \mathbf{u}_{0,h} \text{ and, for almost} \\ \text{every } t \in (0, T), \\ \\ (\partial_t \mathbf{u}_h(t), \mathbf{v}_h)_{\mathbf{L}^2(\Omega)} + k_h(\mathbf{u}_h(t), \mathbf{v}_h) \\ + c(\mathbf{u}_h(t), \mathbf{u}_h(t); \mathbf{v}_h) - b(p_h(t), \mathbf{v}_h) + b(q_h, \mathbf{u}_h(t)) = (\mathbf{f}(t), \mathbf{v}_h)_{\mathbf{L}^2(\Omega)} \\ \\ \text{for all } \mathbf{v}_h \in \mathcal{V}_{0,h} \text{ and } q_h \in \mathcal{Q}_{0,h} \text{ where} \\ \\ b(q, \mathbf{v}) = (q, \text{div} \mathbf{v})_{L^2(\Omega)}, \quad \forall q \in L^2(\Omega), \mathbf{v} \in \mathbf{H}^1(\Omega), \quad (41) \\ c(\mathbf{w}, \mathbf{x}; \mathbf{v}) = -(\mathbf{w} \otimes \mathbf{x}, \nabla \mathbf{v})_{(L^2(\Omega))^{d \times d}}, \quad \forall \mathbf{w}, \mathbf{x}, \mathbf{v} \in \mathbf{H}^1(\Omega). \quad (42) \end{array} \right. \quad (40)$$

We immediately remark that the semi-discrete problem we have obtained is a set of coupled first-order nonlinear ordinary differential equations. As such, we can use standard approaches from the theory of ordinary differential equations to obtain existence, uniqueness, and regularity results. We may also use standard time-integration schemes to obtain a fully-discrete formulation.

We have the following lemma detailing the consistency of our numerical method for sufficiently regular exact solutions.

Lemma 6.1. *Suppose that a Leray-Hopf solution (\mathbf{u}, p) of the homogeneous unsteady Navier-Stokes problem satisfies the regularity conditions*

$$\partial_t \mathbf{u} \in L^2(0, T; \mathbf{L}^2(\Omega)), \quad \mathbf{u} \in L^2(0, T; \mathbf{H}^{3/2+\epsilon}(\Omega))$$

where $\epsilon > 0$. Then, for almost every $t \in (0, T)$:

$$\begin{aligned} (\partial_t \mathbf{u}(t), \mathbf{v}_h)_{\mathbf{L}^2(\Omega)} + k_h(\mathbf{u}(t), \mathbf{v}_h) + c(\mathbf{u}(t), \mathbf{u}(t); \mathbf{v}_h) \\ - b(p(t), \mathbf{v}_h) + b(q_h, \mathbf{u}(t)) = (\mathbf{f}(t), \mathbf{v}_h)_{\mathbf{L}^2(\Omega)} \end{aligned} \quad (43)$$

for all $\mathbf{v}_h \in \mathcal{V}_{0,h}$ and $q_h \in \mathcal{Q}_{0,h}$.

Proof. We trivially have, for almost every $t \in (0, T)$,

$$b(q_h, \mathbf{u}(t)) = 0, \quad \forall q_h \in \mathcal{Q}_{0,h}. \quad (44)$$

Now let $\mathbf{v}_h \in \mathcal{V}_{0,h}$. By the Sobolev trace theorem, our smoothness assumption for \mathbf{u} guarantees that $(\nabla^s \mathbf{u}) \mathbf{n}$ is well-defined along $\partial\Omega$ and belongs to $L^2(0, T; (L^2(\partial\Omega))^d)$. Hence, we can utilize integration by parts and the fact that $\mathbf{u}(t)$ satisfies homogeneous Dirichlet boundary conditions and \mathbf{v}_h satisfies homogeneous normal Dirichlet boundary conditions to write, for almost every $t \in (0, T)$,

$$\begin{aligned} (\partial_t \mathbf{u}(t), \mathbf{v}_h)_{\mathbf{L}^2(\Omega)} + k_h(\mathbf{u}(t), \mathbf{v}_h) + c(\mathbf{u}(t), \mathbf{u}(t); \mathbf{v}_h) - b(p(t), \mathbf{v}_h) \\ = \int_{\Omega} (\partial_t \mathbf{u}(t) - \nabla \cdot (2\nu \nabla^s \mathbf{u}(t)) + \nabla \cdot (\mathbf{u} \otimes \mathbf{u}) + \nabla p(t)) \cdot \mathbf{v}_h \\ = (\mathbf{f}(t), \mathbf{v}_h)_{\mathbf{L}^2(\Omega)}. \end{aligned}$$

This completes the proof of the lemma. \square

We also have the following lemma which is a direct consequence of Proposition 5.3.

Lemma 6.2 (Conservation of mass). *Suppose $(\mathbf{u}_h, p_h) \in \mathcal{V}_T^h \times \mathcal{Q}_T^h$ is a solution to (G). Then*

$$\int_0^T \|\operatorname{div} \mathbf{u}_h(t)\|_{L^2(\Omega)}^2 dt = 0. \quad (45)$$

That is, $\operatorname{div} \mathbf{u}_h = 0$ as a distribution.

Weak imposition of no-slip boundary conditions allows our methodology to automatically default to a compatible semi-discretization of Euler flow in the setting of vanishing viscosity. Moreover, for large Reynolds number flows, there is a sharp boundary layer in the vicinity of walls. Utilizing Nitsche's method allows us to account for these layers in a stable and consistent manner without having to directly resolve them [5, 6, 7]. In fact, Nitsche's method can be interpreted as a variationally consistent wall model. To better see this, let us formally rewrite our semi-discrete variational equations as

$$\begin{aligned} (\partial_t \mathbf{u}_h(t), \mathbf{v}_h)_{\mathbf{L}^2(\Omega)} + \int_{\Omega} \mathbb{T}(t) : \nabla^s \mathbf{v}_h d\mathbf{x} - \sum_{F \in \Gamma_h} \int_F \mathbb{Q}(t) \cdot \mathbf{v}_h ds \\ + c(\mathbf{u}_h(t), \mathbf{u}_h(t); \mathbf{v}_h) - b(p_h(t), \mathbf{v}_h) + b(q_h, \mathbf{u}_h(t)) = (\mathbf{f}(t), \mathbf{v}_h)_{\mathbf{L}^2(\Omega)} \end{aligned} \quad (46)$$

where \mathbb{T} is a symmetric tensor satisfying

$$\begin{aligned} \int_{\Omega} \mathbb{T}(t) : \mathbb{W} d\mathbf{x} &= \int_{\Omega} 2\nu \nabla^s \mathbf{u}_h(t) : \mathbb{W} d\mathbf{x} - \sum_{F \in \Gamma_h} \int_F 2\nu \mathbf{u}_h(t) \cdot (\mathbb{W} \mathbf{n}) ds \\ &= \int_{\Omega} 2\nu \mathbf{u}_h(t) \cdot \operatorname{div} \mathbb{W} d\mathbf{x} \quad (\text{in the sense of distributions}) \end{aligned} \quad (47)$$

for symmetric tensors \mathbb{W} with well-defined normal trace and \mathbb{Q} is a vector satisfying

$$\mathbb{Q}(t) = 2\nu \left((\nabla^s \mathbf{u}_h(t)) \mathbf{n} - \frac{C_{pen}}{h} \mathbf{u}_h(t) \right). \quad (48)$$

Above, \mathbb{T} is a weakly defined viscous stress tensor and \mathbb{Q} is the resultant viscous boundary traction vector. The tangential component of \mathbb{Q} , given by

$$\mathbb{Q}_{tang} = \mathbb{Q} - (\mathbb{Q} \cdot \mathbf{n}) \mathbf{n}, \quad (49)$$

is the *effective wall shear stress vector*. As the semi-discrete velocity field satisfies the no-penetration boundary condition strongly, the vector \mathbb{Q} is equal to the semi-discrete shear stress $2\nu (\nabla^s \mathbf{u}_h) \mathbf{n}$ plus an additional wall shear stress term \mathbb{Q}^+ in the direction tangent to the wall. Specifically, we have

$$\mathbb{Q}^+ = -u^{*2} \frac{\mathbf{u}_h}{\|\mathbf{u}_h\|} \quad (50)$$

where

$$u^{*2} = \frac{2\nu C_{pen} \|\mathbf{u}_h\|}{h}. \quad (51)$$

For under-resolved flow simulations, the magnitude of $(\nabla^s \mathbf{u}_h) \mathbf{n}$ in the direction tangent to the wall is relatively small and, as such, the tangential component of \mathbb{Q} is dominated by \mathbb{Q}^+ . In this sense, \mathbb{Q}^+ becomes a model for the wall shear stress. As the mesh is refined and the flow is resolved, $\mathbb{Q}^+ \rightarrow 0$. The above interpretation allows us to design physically motivated penalty values for Nitsche's penalty parameter. Notably, u^* may be interpreted as the friction velocity. By specifying the value of u^* using Spalding's law of the wall [47], we recover a standard wall model for under-resolved flow simulations. For more on this approach, see Section 3 of [6]. It is important to note, however, that the numerically inspired version, (50), produced results of the same quality as the u^* given by Spalding's physically inspired law of the wall.

Remark 6.1. *If we wish to impose non-homogeneous tangential Dirichlet (e.g., prescribed slip) boundary conditions, we must add the following expression to the right hand side of our semi-discrete formulation:*

$$f_N(\mathbf{v}_h) = \sum_{F \in \Gamma_h} \int_F 2\nu \left(-((\nabla^s \mathbf{v}_h) \mathbf{n}) \cdot \mathbf{u}_{BC}(t) + \frac{C_{pen}}{h_F} \mathbf{u}_{BC}(t) \cdot \mathbf{v}_h \right) ds \quad (52)$$

where \mathbf{u}_{BC} is a prescribed vector function defined on $\partial\Omega$ with prescribed boundary values. If we also wish to impose non-homogeneous normal Dirichlet (e.g., prescribed

penetration) boundary conditions, we must impose these strongly and add the following expression to the left hand side of our semi-discrete formulation:

$$c_{UW}(\mathbf{u}_h(t), \mathbf{v}_h) = \sum_{F \in \Gamma_h} \int_F (\mathbf{u}_{BC}(t) \cdot \mathbf{n})_+ \mathbf{u}_h(t) \cdot \mathbf{v}_h ds \quad (53)$$

and the following expression to the right hand side of our semi-discrete formulation:

$$f_{UW}(\mathbf{v}_h) = - \sum_{F \in \Gamma_h} \int_F (\mathbf{u}_{BC}(t) \cdot \mathbf{n})_- \mathbf{u}_{BC}(t) \cdot \mathbf{v}_h ds \quad (54)$$

where

$$(\mathbf{u}_{BC}(t) \cdot \mathbf{n})_+ = \begin{cases} \mathbf{u}_{BC}(t) \cdot \mathbf{n} & \text{if } \mathbf{u}_{BC}(t) \cdot \mathbf{n} > 0 \\ 0 & \text{otherwise} \end{cases}$$

and

$$(\mathbf{u}_{BC}(t) \cdot \mathbf{n})_- = \begin{cases} \mathbf{u}_{BC}(t) \cdot \mathbf{n} & \text{if } \mathbf{u}_{BC}(t) \cdot \mathbf{n} \leq 0 \\ 0 & \text{otherwise.} \end{cases}$$

These additional terms correspond to upwinding.

6.2 Energy Balance

Our semi-discrete formulation satisfies a discrete energy balance law if we assume that the constant in Nitsche's method is chosen large enough. First, in light of Proposition 5.5, we assume that

$$C_{pen} \geq 4h_K C_{Poin}^2 C_{Korn} \frac{\|(\nabla^s \mathbf{v}_h) \mathbf{n}\|_{(L^2(\partial K))^d}^2}{\|\mathbf{v}_h\|_{\mathbf{H}^1(K)}^2}, \quad \forall K \in \mathcal{K}_h, \mathbf{v}_h \in \mathcal{V}_{0,h} \quad (55)$$

where C_{Poin} is the positive constant appearing in Poincaré's inequality:

$$\|\mathbf{v}\|_{\mathbf{H}^1(\Omega)} \leq C_{Poin} |\mathbf{v}|_{\mathbf{H}^1(\Omega)}, \quad \forall \mathbf{v} \in \mathbf{H}^1(\Omega) \cap \mathbf{H}_0(\text{div}; \Omega)$$

and C_{Korn} is the positive constant associated with the following Korn's inequality [10]:

$$|\mathbf{w}|_{\mathbf{H}^1(\Omega)}^2 \leq C_{Korn} \left(\|\nabla^s \mathbf{w}\|_{(L^2(\Omega))^{d \times d}}^2 + |\partial\Omega|^{-1/(d-1)} \|\mathbf{w}\|_{(L^2(\partial\Omega))^d}^2 \right), \quad \forall \mathbf{w} \in \mathbf{H}^1(\Omega).$$

Second, we assume that

$$C_{pen} \geq 4h_0 |\partial\Omega|^{-1/(d-1)} \quad (56)$$

where h_0 is the mesh size of the coarsest mesh \mathcal{K}_0 and $|\partial\Omega|$ denotes the length of $\partial\Omega$ for $d = 2$ and the area of $\partial\Omega$ for $d = 3$. Assumptions (55) and (56) ensure that the bilinear form $k_h(\cdot, \cdot)$ is coercive (see [22, 23] for details).

Lemma 6.3 (Global balance law for energy). *Suppose $(\mathbf{u}_h, p_h) \in \mathcal{V}_T^h \times \mathcal{Q}_T^h$ is a solution to (G). Furthermore, assume (55) and (56) are satisfied. Then*

$$\frac{1}{2} \frac{d}{dt} \|\mathbf{u}_h(t)\|_{\mathbf{L}^2(\Omega)}^2 = -k_h(\mathbf{u}_h(t), \mathbf{u}_h(t)) + (\mathbf{f}(t), \mathbf{u}_h(t))_{\mathbf{L}^2(\Omega)} \leq (\mathbf{f}(t), \mathbf{u}_h(t))_{\mathbf{L}^2(\Omega)} \quad (57)$$

for almost every $t \in (0, T)$.

Proof. Insert $(\mathbf{v}_h, q_h) = (\mathbf{u}_h(t), 0)$ into (40) for almost every $t \in (0, T)$ and use the fact that $\operatorname{div} \mathbf{u}_h = 0$ as a distribution to obtain the expression

$$(\partial_t \mathbf{u}_h(t), \mathbf{u}_h(t))_{\mathbf{L}^2(\Omega)} + k_h(\mathbf{u}_h(t), \mathbf{u}_h(t)) + c(\mathbf{u}_h(t), \mathbf{u}_h(t); \mathbf{u}_h(t)) = (\mathbf{f}(t), \mathbf{u}_h(t))_{\mathbf{L}^2(\Omega)}.$$

An immediate application of the product rule yields

$$\frac{1}{2} \frac{d}{dt} \|\mathbf{u}_h(t)\|_{\mathbf{L}^2(\Omega)}^2 + k_h(\mathbf{u}_h(t), \mathbf{u}_h(t)) + c(\mathbf{u}_h(t), \mathbf{u}_h(t); \mathbf{u}_h(t)) = (\mathbf{f}(t), \mathbf{u}_h(t))_{\mathbf{L}^2(\Omega)}.$$

To proceed, we write

$$c(\mathbf{u}_h(t), \mathbf{u}_h(t); \mathbf{u}_h(t)) = - \int_{\Omega} (\mathbf{u}_h(t) \otimes \mathbf{u}_h(t)) : \nabla \mathbf{u}_h(t) d\mathbf{x}.$$

Since $\operatorname{div} \mathbf{u}_h = 0$, we have

$$c(\mathbf{u}_h(t), \mathbf{u}_h(t); \mathbf{u}_h(t)) = -\frac{1}{2} \int_{\Omega} \operatorname{div} (\mathbf{u}_h(t) |\mathbf{u}_h(t)|^2) d\mathbf{x},$$

and by the divergence theorem,

$$c(\mathbf{u}_h(t), \mathbf{u}_h(t); \mathbf{u}_h(t)) = 0.$$

To complete the proof, note that $k_h(\cdot, \cdot)$ is coercive due to Corollary 6.2 of [23]. \square

The above energy balance law is analogous to the balance law satisfied by Leray-Hopf weak solutions. However, while we have an equality in our discrete balance law, the balance law for Leray-Hopf weak solutions is characterized by an inequality. This inequality is an artifact of regularization and passing to the limit. Note that when the applied forcing term is conservative (*i.e.*, $\mathbf{f} = \nabla q$ for some scalar potential $q : \Omega \rightarrow \mathbb{R}$), we have

$$\frac{1}{2} \frac{d}{dt} \|\mathbf{u}_h(t)\|_{\mathbf{L}^2(\Omega)}^2 \leq 0$$

for almost every $t \in (0, T)$. Hence, our formulation properly dissipates energy in the presence of conservative forces. Furthermore, when the viscosity is taken to vanish, we obtain

$$\frac{1}{2} \frac{d}{dt} \|\mathbf{u}_h(t)\|_{\mathbf{L}^2(\Omega)}^2 = 0.$$

Thus, just as in the infinite-dimensional setting, energy is an inviscid invariant for our semi-discrete formulation. Consequently, our formulation exhibits time-reversibility.

6.3 Global Existence and Uniqueness

Using standard approaches from the theory of ordinary differential equations, we obtain the following theorem.

Theorem 6.1. *Assume (55) and (56) are satisfied. Then Problem (G) has a unique solution $(\mathbf{u}_h, p_h) \in \mathcal{V}_T^h \times \mathcal{Q}_T^h$. Moreover,*

$$\|\mathbf{u}_h\|_{L^\infty(0, T; \mathbf{L}^2(\Omega))} \leq e^T (\|\mathbf{u}_{0,h}\|_{\mathbf{L}^2(\Omega)} + \|\mathbf{f}\|_{L^2(0, T; \mathbf{L}^2(\Omega))}). \quad (58)$$

Proof. We begin by establishing existence and uniqueness for the semi-discrete velocity solution. To do so, we restrict ourselves to the divergence-free space

$$\mathring{\mathcal{V}}_T^h := \{\mathbf{v}_h \in \mathcal{V}_T^h : \operatorname{div} \mathbf{v}_h = 0\}.$$

Each function $\mathbf{v}_h \in \mathring{\mathcal{V}}_T^h$ can be written uniquely as

$$\mathbf{v}_h(t) = \sum_{i=1}^m e_i(t) \mathbf{w}_i$$

where $\{\mathbf{w}_i\}_{i=1}^m$ is a basis for the space

$$\mathring{\mathcal{V}}_{0,h} := \{\mathbf{w}_h \in \mathcal{V}_{0,h} : \operatorname{div} \mathbf{w}_h = 0\}.$$

Representing our desired solution as

$$\mathbf{u}_h(t) = \sum_{i=1}^m d_i(t) \mathbf{w}_i,$$

the semi-discrete problem in the kernel becomes a nonlinear system of first-order ordinary differential equations for the coefficients $d_i(t)$ subject to appropriately defined initial conditions. The energy estimate in Lemma 6.3 can then be used in conjunction with Gronwall's inequality to show that there exists a unique absolutely continuous function $\mathbf{d}(t) = (d_1(t), \dots, d_m(t))$ such that the initial conditions are satisfied and the nonlinear system of first-order ordinary differential equations is satisfied for almost every time $t \in (0, T)$. Hence, a solution $\mathbf{u}_h \in \mathring{\mathcal{V}}_T^h$ exists and is unique. Existence and uniqueness of $p_h \in \mathcal{Q}_T^h$ is an immediate consequence of the inf-sup condition for the bilinear form $b(\cdot, \cdot)$. To obtain the L^2 stability estimate, we write using Lemma 6.3

$$\frac{d}{dt} \|\mathbf{u}_h(t)\|_{\mathbf{L}^2(\Omega)}^2 \leq 2(\mathbf{f}(t), \mathbf{u}_h(t))_{\mathbf{L}^2(\Omega)} \leq \|\mathbf{f}(t)\|_{\mathbf{L}^2(\Omega)}^2 + \|\mathbf{u}_h(t)\|_{\mathbf{L}^2(\Omega)}^2$$

for almost every $t \in (0, T)$. The desired estimate is then an immediate result of the differential form of Gronwall's inequality. \square

Note that the above theorem gives existence and uniqueness results for any end-time T . Hence, we have global-in-time existence and uniqueness for our semi-discrete problem. Moreover, our method is well-posed in the sense that it returns semi-discrete solutions which depend continuously on the given data. This gives our methodology firm mathematical grounding.

6.4 *A Priori* Error Estimates

If one assumes that a Leray-Hopf solution to the unsteady Navier-Stokes equations is sufficiently smooth, one can use standard functional analysis techniques to prove our semi-discrete velocity solution converges at optimal order (with respect to the mesh size) to the Leray-Hopf velocity solution. The main idea is due to Heywood and

Rannacher [26] and involves splitting the velocity error into two components: an error contribution associated with the semi-discrete solution of a linearized unsteady Stokes problem and a remainder term comprising the difference between the semi-discrete Stokes solution and the semi-discrete Navier-Stokes solution. The resulting analysis is lengthy, tedious, and tangential, and, as such, we have elected not to include it here. The final *a priori* estimate is reported in the theorem below, and the interested reader is directed to Chapter 9 of [19].

Theorem 6.2. *Assume that (55) and (56) are satisfied and that the domain Ω satisfies the elliptic regularity condition. Let \mathbf{u} denote a Leray-Hopf solution of the unsteady Navier-Stokes equations and (\mathbf{u}_h, p_h) denote the unique weak solution of (G). If the regularity conditions*

$$\mathbf{u} \in L^\infty(0, T; \mathbf{H}^{j+1}(\Omega)), \quad \partial_t \mathbf{u} \in L^2(0, T; \mathbf{H}^{j+1}(\Omega))$$

hold for $j \geq 1$, then we have

$$\begin{aligned} & \|\mathbf{u} - \mathbf{u}_h\|_{L^\infty(0, T; \mathbf{L}^2(\Omega))}^2 \leq \\ & C_{NS} (1 + QT \exp\{\beta T\}) h^{2(s+1)} \left(\|\mathbf{u}\|_{L^\infty(0, T; \mathbf{H}^{s+1}(\Omega))}^2 + (2\nu)^{-1} \|\partial_t \mathbf{u}\|_{L^2(0, T; \mathbf{H}^{s+1}(\Omega))}^2 \right) \end{aligned} \quad (59)$$

where $s = \min\{k', j\}$, Q and β are positive constants independent of h and T that scale asymptotically with ν^{-1} and depend on the supremum of \mathbf{u} over $\Omega \times [0, T)$, and C_{NS} is a positive constant independent of h , ν , and T that scales asymptotically with C_{pen} .

Note that while the above theorem gives an optimal \mathbf{L}^2 error bound for the velocity field in terms of the mesh size h , the bound grows exponentially in time. In general, such a dependence is unavoidable. However, if we assume an exact solution is stable in the sense that perturbations decay exponentially in time, we can use standard techniques to prove error estimates which are uniform in time [27]. Furthermore, it is known that solutions of the unsteady Navier-Stokes problem may experience blow up at the initial time unless certain compatibility conditions relating the initial condition and applied forcing are satisfied. The inherent smoothing properties of unsteady Navier-Stokes flow may be exploited in order to derive optimal error estimates away from the initial time for higher-order spatial discretizations [28]. Finally, an additional analysis can be conducted to obtain error estimates which are suboptimal, by one order, for the semi-discrete pressure field. Our numerical experience has suggested that the semi-discrete pressure field converges at optimal order in contrast with these estimates.

7 Balance Laws

In this section, we present a collection of balance laws for our semi-discretization scheme. These balance laws supplement the discrete energy balance law derived in

Subsection 6.2 and give our semi-discrete formulation geometric structure. Before proceeding further, we pose our semi-discrete problem in a slightly different form. This form will more directly reveal the conservation structure of our chosen semi-discretization. Let us introduce the following discrete trace space:

$$\mathcal{V}_{trace,h} := \{q \in L^2(\partial\Omega) : q = \mathbf{v}_h \cdot \mathbf{n}, \mathbf{v}_h \in \mathcal{V}_h\}. \quad (60)$$

Note that, in the above expression, \mathcal{V}_h denotes the space of discrete velocity fields which are free of Dirichlet boundary conditions. $\mathcal{V}_{trace,h}$ represents the natural trace space associated with \mathcal{V}_h , and it is a Hilbert space when endowed with the standard L^2 inner-product over $\partial\Omega$. Introducing the space-time trace space

$$\mathcal{V}_{trace,T}^h := L^2(0, T; \mathcal{V}_{trace,h}), \quad (61)$$

let us consider the following semi-discrete problem.

$$(A) \left\{ \begin{array}{l} \text{Find } \mathbf{u}_h \in \mathcal{V}_T^h, p_h \in \mathcal{Q}_T^h, \text{ and } p_{trace,h} \in \mathcal{V}_{trace,T}^h \text{ such that } \mathbf{u}_h(0) = \mathbf{u}_{0,h} \\ \text{and, for almost every } t \in (0, T), \\ \\ (\partial_t \mathbf{u}_h(t), \mathbf{v}_h)_{\mathbf{L}^2(\Omega)} + k_h(\mathbf{u}_h(t), \mathbf{v}_h) + c(\mathbf{u}_h(t), \mathbf{u}_h(t); \mathbf{v}_h) \\ - b(p_h(t), \mathbf{v}_h) + (p_{trace,h}(t), \mathbf{v}_h \cdot \mathbf{n})_{L^2(\partial\Omega)} + b(q_h, \mathbf{u}_h(t)) = (\mathbf{f}(t), \mathbf{v}_h)_{\mathbf{L}^2(\Omega)} \\ \\ \text{for all } \mathbf{v}_h \in \mathcal{V}_h \text{ and } q_h \in \mathcal{Q}_{0,h}. \end{array} \right. \quad (62)$$

Here, we have introduced the auxiliary field $p_{trace,h}$ and released the no-penetration boundary condition on the discrete test space for the momentum equations. Note that the solution of Problem (G) is also a solution to Problem (A) (modulo the auxiliary field $p_{trace,h}$) since

$$(p_{trace,h}(t), \mathbf{v}_h \cdot \mathbf{n})_{L^2(\partial\Omega)} = 0, \quad \forall \mathbf{v}_h \in \mathcal{V}_{0,h}.$$

Furthermore, the auxiliary field $p_{trace,h}$ is unique due to the obvious inf-sup condition

$$\inf_{\substack{q_h \in \mathcal{V}_{trace,h} \\ q_h \neq 0}} \sup_{\mathbf{v}_h \in \mathcal{V}_h} (q_h, \mathbf{v}_h \cdot \mathbf{n})_{L^2(\partial\Omega)} = \|q_h\|_{L^2(\partial\Omega)}^2.$$

By employing integration by parts, we observe the auxiliary field $p_{trace,h}$ approximates the trace of the pressure field. Hence, $p_{trace,h} \mathbf{n}$ gives the semi-discrete normal traction on $\partial\Omega$ due to pressure forces.

7.1 Conservation Properties on Rectilinear Domains

Suppose that Ω is a rectilinear domain that has been mapped from parametric space using an affine transformation. Then, the unit vectors $\mathbf{e}_i \in \mathbb{R}^d$ necessarily belong to the discrete space \mathcal{V}_h . If we select $\mathbf{v}_h = \mathbf{e}_i$ and $q_h = p_h(t)$ in (62) and sum over $i = 1, \dots, d$, we obtain the following discrete balance law for linear momentum.

Global conservation of linear momentum on rectilinear domains. For rectilinear domains, the semi-discrete velocity field \mathbf{u}_h satisfies

$$\frac{d}{dt} \int_{\Omega} \mathbf{u}_h(t) d\mathbf{x} = \int_{\partial\Omega} (-p_{trace,h}(t) \mathbf{n} + \mathbb{Q}(t)) ds + \int_{\Omega} \mathbf{f}(t) d\mathbf{x} \quad (63)$$

for almost all $t \in (0, T)$ where

$$\mathbb{Q}(t) = 2\nu \left((\nabla^s \mathbf{u}_h(t)) \mathbf{n} - \frac{C_{pen}}{h_F} \mathbf{u}_h(t) \right)$$

for a given mesh face $F \in \Gamma_h$.

By interpreting Nitsche's method as a variational wall model as was discussed in Subsection 6.1, we see that the above balance law dictates that linear momentum enters or leaves the system either through body forces or surface traction forces. Hence, our semi-discrete formulation properly mimics the continuous problem. We can derive similar balance laws when non-homogeneous Dirichlet, traction, or periodic boundary conditions are specified instead of homogeneous Dirichlet boundary conditions. Additionally, we can derive momentum balance laws over subdomains by introducing auxiliary flux spaces on subdomain boundaries. For more on this procedure, see [31].

7.2 Conservation Properties on Cylindrical Domains

When the domain Ω is not rectilinear, our semi-discrete formulation is no longer guaranteed to globally conserve linear momentum. This is because the Piola transformation does not, in general, map constant vector fields in parametric space to constant vector fields in physical space. However, the special structure of the Piola transformation allows our formulation to admit more natural momentum balance laws for general parametric domains. In this subsection, we demonstrate that if Ω is a cylindrical domain defined via a polar mapping, our formulation globally conserves axial angular momentum and axial linear momentum.

To proceed, let us introduce the mapping

$$\mathbf{F}(\xi_1, \xi_2, \xi_3) = \begin{bmatrix} ((r_{out} - r_{in})\xi_2 + r_{in}) \sin(2\pi\xi_1) \\ ((r_{out} - r_{in})\xi_2 + r_{in}) \cos(2\pi\xi_1) \\ H\xi_3 \end{bmatrix}, \forall (\xi_1, \xi_2, \xi_3) \in (0, 1)^3$$

from the parametric domain $\widehat{\Omega} = (0, 1)^3$ to a physical domain Ω set between two concentric cylinders. The radius of the inner cylinder is taken to be r_{in} , the radius of the outer cylinder is taken to be r_{out} , and the heights of the cylinders are taken to be H . Periodicity is applied in the ξ_1 direction. We have the following relationship between our parametric coordinate system and the cylindrical coordinate system (θ, r, z) :

$$\begin{aligned} \theta &= 2\pi\xi_1 \\ r &= (r_{out} - r_{in})\xi_2 + r_{in} \\ z &= H\xi_3. \end{aligned}$$

Without loss of generality, let us assume that $r_{in} = 1$, $r_{out} = 2$, and $H = 1$. The semi-discrete velocity functions $\mathbf{v}_h \in \mathcal{V}_h$ have the representation

$$\mathbf{v}_h(\mathbf{x}(\boldsymbol{\xi})) := \frac{1}{\det(D\mathbf{F}(\boldsymbol{\xi}))} D\mathbf{F}(\boldsymbol{\xi}) \widehat{\mathbf{v}}_h(\boldsymbol{\xi})$$

where $\widehat{\mathbf{v}}_h \in \widehat{\mathcal{V}}_h$. A direct computation shows

$$\mathbf{v}_h(\mathbf{x}(\boldsymbol{\xi})) := \begin{bmatrix} \cos(\theta) & \frac{\sin(\theta)}{2\pi r} & 0 \\ -\sin(\theta) & \frac{\cos(\theta)}{2\pi r} & 0 \\ 0 & 0 & \frac{1}{2\pi r} \end{bmatrix} \widehat{\mathbf{v}}_h(\boldsymbol{\xi}).$$

Now, since the space $\widehat{\mathcal{V}}_h$ contains all vector-valued functions which are linear polynomials in ξ_1 , ξ_2 , and ξ_3 (since $k' \geq 1$), we have thus proven the vector-valued functions

$$\mathbf{s} = \begin{bmatrix} \cos(\theta) & \frac{\sin(\theta)}{2\pi r} & 0 \\ -\sin(\theta) & \frac{\cos(\theta)}{2\pi r} & 0 \\ 0 & 0 & \frac{1}{2\pi r} \end{bmatrix} \begin{bmatrix} r \\ 0 \\ 0 \end{bmatrix} = \begin{bmatrix} r \cos(\theta) \\ -r \sin(\theta) \\ 0 \end{bmatrix} = \begin{bmatrix} y \\ -x \\ 0 \end{bmatrix}$$

and

$$\mathbf{z} = \begin{bmatrix} \cos(\theta) & \frac{\sin(\theta)}{2\pi r} & 0 \\ -\sin(\theta) & \frac{\cos(\theta)}{2\pi r} & 0 \\ 0 & 0 & \frac{1}{2\pi r} \end{bmatrix} \begin{bmatrix} 0 \\ 0 \\ 2\pi r \end{bmatrix} = \begin{bmatrix} 0 \\ 0 \\ 1 \end{bmatrix}$$

are members of \mathcal{V}_h . Let us now select $\mathbf{v}_h = \mathbf{s}$ and $q_h = p_h(t)$ in (62). Since

$$\nabla \mathbf{s} = \begin{bmatrix} 0 & 1 & 0 \\ -1 & 0 & 0 \\ 0 & 0 & 0 \end{bmatrix}$$

is an anti-symmetric matrix, we have

$$\begin{aligned} \int_{\Omega} (2\nu (\nabla^s \mathbf{u}_h(t)) : (\nabla^s \mathbf{s}) - (\mathbf{u}_h(t) \otimes \mathbf{u}_h(t)) : \nabla \mathbf{s}) \, d\mathbf{x} \\ - \int_{\partial\Omega} 2\nu ((\nabla^s \mathbf{s}) \mathbf{n}) \cdot \mathbf{u}_h(t) \, ds = 0 \end{aligned}$$

for almost every $t \in (0, T)$. Therefore,

$$\begin{aligned} \frac{d}{dt} \int_{\Omega} \mathbf{u}_h(t) \cdot \mathbf{s} \, d\mathbf{x} &= \int_{\partial\Omega} \left(-p_{trace,h}(t) \mathbf{n} + 2\nu \left((\nabla^s \mathbf{u}_h(t)) \mathbf{n} - \frac{C_{pen}}{h_F} \mathbf{u}_h(t) \right) \right) \cdot \mathbf{s} \, ds \\ &+ \int_{\Omega} \mathbf{f}(t) \cdot \mathbf{s} \, d\mathbf{x}. \end{aligned}$$

Furthermore, we have that

$$\mathbf{w} \cdot \mathbf{s} = (\mathbf{w} \times \mathbf{r})_z, \quad \forall \mathbf{w} \in \mathbb{R}^3$$

where $(\cdot)_z$ denotes the z -component of a vector and

$$\mathbf{r} = \begin{bmatrix} r \sin(\theta) \\ r \cos(\theta) \\ 0 \end{bmatrix}.$$

Hence, we have proven the following balance law for axial angular momentum.

Global conservation of axial angular momentum on cylindrical domains.

For cylindrical domains, the semi-discrete velocity field \mathbf{u}_h satisfies

$$\begin{aligned} \frac{d}{dt} \int_{\Omega} (\mathbf{u}_h(t) \times \mathbf{r})_z \, d\mathbf{x} &= \int_{\partial\Omega} ((-p_{trace,h}(t)\mathbf{n} + \mathbb{Q}(t)) \times \mathbf{r})_z \, ds \\ &+ \int_{\Omega} (\mathbf{f}(t) \times \mathbf{r})_z \, d\mathbf{x} \end{aligned} \quad (64)$$

for almost all $t \in (0, T)$ where

$$\mathbf{r} = \begin{bmatrix} r \sin(\theta) \\ r \cos(\theta) \\ 0 \end{bmatrix}$$

and

$$\mathbb{Q}(t) = 2\nu \left((\nabla^s \mathbf{u}_h(t)) \mathbf{n} - \frac{C_{pen}}{h_F} \mathbf{u}_h(t) \right)$$

for a given mesh face $F \in \Gamma_h$.

The above balance law dictates that axial angular momentum enters or leaves the semi-discrete system either through applied moments or torques. This balance law mimics the corresponding continuous balance law for axial angular momentum. We would like to mention that derivation of this balance law was contingent upon employing the symmetrized gradient for the viscous stress term instead of the full gradient.

Selecting $\mathbf{v}_h = \mathbf{z}$ and $q_h = p_h(t)$ in (62) yields the following balance law for axial linear momentum. It states that axial momentum enters or leaves the system either through axial body forces or axial traction forces.

Global conservation of axial linear momentum on cylindrical domains. *For cylindrical domains, the semi-discrete velocity field \mathbf{u}_h satisfies*

$$\begin{aligned} \frac{d}{dt} \int_{\Omega} (\mathbf{u}_h(t))_z \, d\mathbf{x} &= \int_{\partial\Omega} ((-p_{trace,h}(t)\mathbf{n} + \mathbb{Q}(t)))_z \, ds \\ &+ \int_{\Omega} (\mathbf{f}(t))_z \, d\mathbf{x} \end{aligned} \quad (65)$$

for almost all $t \in (0, T)$ where

$$\mathbb{Q}(t) = 2\nu \left((\nabla^s \mathbf{u}_h(t)) \mathbf{n} - \frac{C_{pen}}{h_F} \mathbf{u}_h(t) \right)$$

for a given mesh face $F \in \Gamma_h$.

As a final note, we would like to state that if we had utilized a NURBS mapping to represent the physical domain Ω , we would have arrived at a global conservation statement for axial angular momentum but not for axial linear momentum. Hence, we believe polar mappings hold a distinct advantage over NURBS mappings when solving problems harboring important symmetry and conservation properties. This being said, we would like to mention that one recovers both linear and angular momentum balance laws when employing NURBS-based isogeometric analysis in conjunction with a residual-based Variational Multiscale method [3]. Such a discretization, however, does not exactly replicate the incompressibility constraint and alternatively attempts to model the effects of fine-scale solution features (including, in this case, compressibility) on the resolved components of the flow.

7.3 Vorticity, Enstrophy, and Helicity

We continue this section by deriving discrete balance laws for vorticity, enstrophy, and helicity when the applied forcing term is conservative (*i.e.*, when the forcing is derived through a potential). In order to do so, we must properly define vorticity at the semi-discrete level (see, for example, [43]). We restrict our discussion to the three-dimensional setting for the remainder of this section. Recall that the vorticity field

$$\boldsymbol{\omega} = \mathbf{curl} \mathbf{u}$$

satisfies the partial differential equations

$$\frac{\partial \boldsymbol{\omega}}{\partial t} + \nabla \cdot (\mathbf{u} \otimes \boldsymbol{\omega} - \boldsymbol{\omega} \otimes \mathbf{u}) = \nabla \cdot (2\nu \nabla^s \boldsymbol{\omega}) \quad (66)$$

and

$$\operatorname{div} \boldsymbol{\omega} = 0 \quad (67)$$

when the applied forcing term is conservative. Furthermore, since $\mathbf{u} = \mathbf{0}$ on $\partial\Omega$,

$$\boldsymbol{\omega} \cdot \mathbf{n} = 0. \quad (68)$$

In light of these identities, conservation statements, and boundary conditions, we define semi-discrete vorticity as the solution of the following problem: find $\boldsymbol{\omega}_h \in \mathring{\mathcal{V}}_T^h = \{\mathbf{v}_h \in \mathcal{V}_T^h : \operatorname{div} \mathbf{v}_h = 0\}$ such that $\boldsymbol{\omega}_h(0) = \boldsymbol{\omega}_{0,h}$ and

$$\begin{aligned} & (\partial_t \boldsymbol{\omega}_h(t), \mathbf{v}_h)_{\mathbf{L}^2(\Omega)} + k_h(\boldsymbol{\omega}_h(t), \mathbf{v}_h) + c(\mathbf{u}_h(t), \boldsymbol{\omega}_h(t); \mathbf{v}_h) - c(\boldsymbol{\omega}_h(t), \mathbf{u}_h(t); \mathbf{v}_h) \\ & = \sum_{F \in \Gamma_h} \int_F 2\nu \left(-((\nabla^s \mathbf{v}_h) \mathbf{n}) \cdot \mathbf{curl} \mathbf{u}_h(t) + \frac{C_{pen}}{h_F} \mathbf{curl} \mathbf{u}_h(t) \cdot \mathbf{v}_h \right) ds \end{aligned} \quad (69)$$

for almost every $t \in (0, T)$ and for all $\mathbf{v}_h \in \mathring{\mathcal{V}}_{0,h}$ where $\boldsymbol{\omega}_{0,h} \in \mathring{\mathcal{V}}_{0,h}$ is a suitably defined initial condition. Note that we have strongly enforced normal boundary conditions for the semi-discrete vorticity field and weakly enforced tangential boundary conditions

using Nitsche's method. It should be further noted that the semi-discrete problem given by (69) may not have a global-in-time solution. This is due to the presence of vortex stretching. However, Picard's existence theorem can be used to show the problem has a unique local-in-time solution. Hence, let us assume for the remainder of this discussion that the end-time T has been sufficiently chosen such that the semi-discrete vorticity equation has a unique solution. Beyond such T , the semi-discrete vorticity may, in theory, experience blow-up. Such a hypothetical blow-up lies at the heart of the Navier-Stokes Millenium Problem.

We now present a discrete balance law for vorticity which holds for periodic domains. It is a simple consequence of choosing $\mathbf{v}_h = \mathbf{e}_i$ in (69) where \mathbf{e}_i is a unit vector. Analogous balance laws can be proven for rectilinear domains subject to no-penetration and no-slip boundary conditions.

Global balance law for vorticity. *Suppose Ω is the three-dimensional torus. For conservative applied forces, the semi-discrete vorticity field $\boldsymbol{\omega}_h$ satisfies*

$$\frac{d}{dt} \int_{\Omega} \boldsymbol{\omega}_h(t) d\mathbf{x} = \mathbf{0} \quad (70)$$

for almost all $t \in (0, T)$.

We next derive a discrete balance law for enstrophy. To begin, we insert $\mathbf{v}_h = \boldsymbol{\omega}_h(t)$ into (69) for almost every $t \in (0, T)$:

$$\begin{aligned} & (\partial_t \boldsymbol{\omega}_h(t), \boldsymbol{\omega}_h(t))_{\mathbf{L}^2(\Omega)} + k_h(\boldsymbol{\omega}_h(t), \boldsymbol{\omega}_h(t)) + c(\mathbf{u}_h(t), \boldsymbol{\omega}_h(t); \boldsymbol{\omega}_h(t)) - c(\boldsymbol{\omega}_h(t), \mathbf{u}_h(t); \boldsymbol{\omega}_h(t)) \\ &= \sum_{F \in \Gamma_h} \int_F 2\nu \left(-((\nabla^s \boldsymbol{\omega}_h(t)) \mathbf{n}) \cdot \mathbf{curl} \mathbf{u}_h(t) + \frac{C_{pen}}{h_F} \mathbf{curl} \mathbf{u}_h(t) \cdot \boldsymbol{\omega}_h(t) \right) ds. \end{aligned}$$

A straight-forward calculation invoking the divergence theorem and taking advantage of the fact that the semi-discrete velocity field is divergence-free yields

$$c(\mathbf{u}_h(t), \boldsymbol{\omega}_h(t); \boldsymbol{\omega}_h(t)) = 0. \quad (71)$$

The product rule gives

$$(\partial_t \boldsymbol{\omega}_h(t), \boldsymbol{\omega}_h(t))_{\mathbf{L}^2(\Omega)} = \frac{d}{dt} \int_{\Omega} \gamma_h(t) d\mathbf{x}$$

where $\gamma_h(t) = \frac{1}{2} |\boldsymbol{\omega}_h(t)|^2$ is the semi-discrete enstrophy density of the fluid. To handle the term corresponding to vortex stretching, we employ integration by parts and the fact that $\text{div} \boldsymbol{\omega}_h = 0$ to write

$$c(\boldsymbol{\omega}_h(t), \mathbf{u}_h(t); \boldsymbol{\omega}_h(t)) = - \int_{\Omega} \boldsymbol{\omega}_h(t)^T \nabla \mathbf{u}(t) \boldsymbol{\omega}_h(t) d\mathbf{x}.$$

A direct calculation then gives

$$\boldsymbol{\omega}_h(t)^T \nabla \mathbf{u}(t) \boldsymbol{\omega}_h(t) = \boldsymbol{\omega}_h(t)^T \mathbb{D}(\mathbf{u}_h(t)) \boldsymbol{\omega}_h(t)$$

where $\mathbb{D}(\mathbf{u}_h(t)) = \nabla^s \mathbf{u}_h(t)$ is the semi-discrete rate of strain tensor. Thus, we have arrived at the following balance law.

Global balance law for enstrophy. *For conservative applied forces, the semi-discrete vorticity field $\boldsymbol{\omega}_h$ satisfies*

$$\begin{aligned} \frac{d}{dt} \int_{\Omega} \gamma_h(t) d\mathbf{x} &= - \int_{\Omega} 2\nu |\nabla^s \boldsymbol{\omega}_h(t)|^2 d\mathbf{x} + \int_{\Omega} \boldsymbol{\omega}_h(t)^T \mathbb{D}(\mathbf{u}_h(t)) \boldsymbol{\omega}_h(t) d\mathbf{x} \\ &+ \int_{\partial\Omega} 2\nu ((\nabla^s \boldsymbol{\omega}_h(t)) \mathbf{n}) \cdot \boldsymbol{\omega}_h(t) ds \\ &+ \sum_{F \in \Gamma_h} \int_F 2\nu \left((\nabla^s \boldsymbol{\omega}_h(t)) \mathbf{n} - \frac{C_{pen}}{h_F} \boldsymbol{\omega}_h(t) \right) \cdot (\boldsymbol{\omega}_h(t) - \mathbf{curl} \mathbf{u}_h(t)) ds \end{aligned} \quad (72)$$

for almost all $t \in (0, T)$.

The first and second lines of (72) contain enstrophy production terms associated with the domain interior and boundary respectively while the third line of (72) contains supplemental production terms associated with weak enforcement of boundary conditions. When the boundary condition

$$\boldsymbol{\omega}_h = \mathbf{curl} \mathbf{u}_h$$

is met exactly, the third line of (72) vanishes and we recover the same entropy balance law as satisfied by the exact vorticity field. Note that since the divergence of \mathbf{u}_h is precisely zero, $\mathbb{D}(\mathbf{u}_h(t))$ has the same indefinite structure as its continuous counterpart. That is, it has three real eigenvalues which sum to zero. Consequently, we have appropriately captured the vortex stretching term with our semi-discrete formulation. The same cannot be said for semi-discretizations which satisfy the incompressibility constraint only approximately, even if the momentum and vorticity equations are written in skew-symmetric form.

We finish here by deriving a discrete balance law for helicity. First insert $(\mathbf{v}_h, q_h) = (\boldsymbol{\omega}_h(t), p_h(t))$ into (40) and $\mathbf{v}_h = \mathbf{u}_h(t)$ into (69) for almost every $t \in (0, T)$. Adding the two resulting expressions and taking into consideration the fact that \mathbf{f} is conservative, we obtain

$$\begin{aligned} &(\partial_t \mathbf{u}_h(t), \boldsymbol{\omega}_h(t))_{\mathbf{L}^2(\Omega)} + k_h(\mathbf{u}_h(t), \boldsymbol{\omega}_h(t)) + c(\mathbf{u}_h(t), \mathbf{u}_h(t); \boldsymbol{\omega}_h(t)) \\ &+ (\partial_t \boldsymbol{\omega}_h(t), \mathbf{u}_h(t))_{\mathbf{L}^2(\Omega)} + k_h(\boldsymbol{\omega}_h(t), \mathbf{u}_h(t)) + c(\mathbf{u}_h(t), \boldsymbol{\omega}_h(t); \mathbf{u}_h(t)) - c(\boldsymbol{\omega}_h(t), \mathbf{u}_h(t); \mathbf{u}_h(t)) \\ &= \sum_{F \in \Gamma_h} \int_F 2\nu \left(-((\nabla^s \mathbf{u}_h(t)) \mathbf{n}) \cdot \mathbf{curl} \mathbf{u}_h(t) + \frac{C_{pen}}{h_F} \mathbf{curl} \mathbf{u}_h(t) \cdot \mathbf{u}_h(t) \right) ds. \end{aligned}$$

By the product rule, we have

$$(\partial_t \mathbf{u}_h(t), \boldsymbol{\omega}_h(t))_{\mathbf{L}^2(\Omega)} + (\partial_t \boldsymbol{\omega}_h(t), \mathbf{u}_h(t))_{\mathbf{L}^2(\Omega)} = \frac{d}{dt} \int_{\Omega} \varrho_h(t) d\mathbf{x}$$

where $\varrho_h(t) = \boldsymbol{\omega}_h(t) \cdot \mathbf{u}_h(t)$ is the semi-discrete helical density of the flow. Integration by parts and the fact that our semi-discrete velocity field is divergence-free give

$$c(\mathbf{u}_h(t), \mathbf{u}_h(t); \boldsymbol{\omega}_h(t)) = -c(\mathbf{u}_h(t), \boldsymbol{\omega}_h(t); \mathbf{u}_h(t)).$$

Finally, a straight-forward calculation invoking the divergence theorem and taking advantage of the fact that the semi-discrete vorticity field is divergence-free yields

$$c(\boldsymbol{\omega}_h(t), \mathbf{u}_h(t); \mathbf{u}_h(t)) = 0.$$

Collecting our equations, we acquire the following balance law for helicity.

Global balance law for helicity. *For conservative applied forces, the semi-discrete solution satisfies*

$$\begin{aligned} \frac{d}{dt} \int_{\Omega} \varrho_h(t) d\mathbf{x} &= - \int_{\Omega} 4\nu (\nabla^s \boldsymbol{\omega}_h(t)) : (\nabla^s \mathbf{u}_h(t)) d\mathbf{x} \\ &+ \int_{\partial\Omega} 2\nu ((\nabla^s \mathbf{u}_h(t)) \mathbf{n}) \cdot \boldsymbol{\omega}_h(t) ds \\ &+ \int_{\partial\Omega} 2\nu ((\nabla^s \boldsymbol{\omega}_h(t)) \mathbf{n}) \cdot \mathbf{u}_h(t) ds \\ &+ \sum_{F \in \Gamma_h} \int_F 2\nu \left((\nabla^s \boldsymbol{\omega}_h(t)) \mathbf{n} - \frac{C_{pen}}{h_F} \boldsymbol{\omega}_h(t) \right) \cdot \mathbf{u}_h(t) ds \\ &+ \sum_{F \in \Gamma_h} \int_F 2\nu \left((\nabla^s \mathbf{u}_h(t)) \mathbf{n} - \frac{C_{pen}}{h_F} \mathbf{u}_h(t) \right) \cdot (\boldsymbol{\omega}_h(t) - \mathbf{curl} \mathbf{u}_h(t)) ds \end{aligned} \tag{73}$$

for almost all $t \in (0, T)$.

The first line of (73) contains helicity production terms associated with the domain interior, the second and third lines of (73) contain production terms associated with the domain boundary, and the fourth and fifth lines of (72) contain supplemental production terms associated with weak enforcement of boundary conditions. When the boundary conditions

$$\mathbf{u}_h = 0$$

and

$$\boldsymbol{\omega}_h = \mathbf{curl} \mathbf{u}_h$$

are met exactly, the fourth and fifth lines of (73) vanish and we recover the same helicity balance law as satisfied by the exact vorticity field.

Note that in the limit of vanishing viscosity our global helicity balance reduces to

$$\frac{d}{dt} \int_{\Omega} \varrho_h(t) d\mathbf{x} = 0.$$

Thus, just as in the infinite-dimensional setting, helicity is an inviscid invariant for our semi-discrete formulation. We believe this is a very important property given the

pivotal role helicity plays in flow structure development. As a final remark, we would like to mention all of the discrete balance laws presented here generalize to other sets of boundary conditions including non-homogeneous Dirichlet boundary conditions, prescribed traction boundary conditions, and periodic boundary conditions.

8 Numerical Experiments

In this section, we numerically test our semi-discretization scheme using three selected benchmark problems: two-dimensional Taylor-Green vortex flow, alternating cylindrical Couette flow, and three-dimensional Taylor-Green vortex flow. Throughout, we choose Nitsche's penalty constant as

$$C_{pen} = 5(k' + 1)$$

which we have found to be sufficiently large in order to ensure numerical stability. Additionally, we employ uniform parametric meshes and B-spline spaces of maximal continuity.

8.1 Two-Dimensional Taylor-Green Vortex Flow

As a first numerical experiment, we consider two-dimensional Taylor-Green vortex flow. Two-dimensional Taylor-Green vortex flow is a simple periodic (in space) vortical flow subject to the initial condition

$$\mathbf{u}_0(x, y) = \begin{bmatrix} \sin(x) \cos(y) \\ -\cos(x) \sin(y) \end{bmatrix}.$$

The exact solution for this flow exponentially decays in time and satisfies the relationships

$$\begin{aligned} \mathbf{u}(x, y, t) &= \begin{bmatrix} \sin(x) \cos(y) \\ -\cos(x) \sin(y) \end{bmatrix} \exp(-2\nu t), \\ p(x, y, t) &= \frac{1}{4} (\cos(2x) + \cos(2y)) \exp(-4\nu t). \end{aligned}$$

It is easily seen that the nonlinear convection term is exactly balanced by the pressure term and thus does not interfere with the evolution of the velocity flow field. Hence, a question of practical interest is whether or not the nonlinear convection term interferes with the evolution of the velocity field at the discrete level.

We have simulated two-dimensional Taylor-Green vortex flow using divergence-conforming B-spline discretizations of varying mesh size and polynomial degree. We restricted our computations to the domain $\Omega = (0, \pi)^2$ by employing symmetry conditions along $\partial\Omega$. A linear parametric mapping was utilized to describe the physical domain. The Crank-Nicolson method [16] was employed to discretize in time, and the time-step size was chosen to be

$$\Delta t = \min \left\{ h^{\frac{k'+1}{2}}, \frac{h^2}{4\nu} \right\},$$

Table 1: Two-dimensional Taylor-Green vortex flow: Convergence rates at $t = 15$ for $Re = 100$. Time-step size chosen as $\Delta t = \min \left\{ h^{\frac{k'+1}{2}}, \frac{h^2}{4\nu} \right\}$.

Polynomial degree $k' = 1$

h	1/8	1/16	1/32	1/64
$ \mathbf{u} - \mathbf{u}_h _{\mathbf{H}^1(\Omega)}$	1.87e-1	9.34e-2	4.67e-2	2.34e-2
order	-	1.00	1.00	1.00
$\ \mathbf{u} - \mathbf{u}_h\ _{\mathbf{L}^2(\Omega)}$	1.02e-2	2.51e-3	6.24e-4	1.56e-4
order	-	2.02	2.01	2.00
$\ p - p_h\ _{L^2(\Omega)}$	1.09e-2	2.57e-3	6.32e-4	1.59e-4
order	-	2.08	2.02	1.99

Polynomial degree $k' = 2$

h	1/8	1/16	1/32	1/64
$ \mathbf{u} - \mathbf{u}_h _{\mathbf{H}^1(\Omega)}$	9.64e-3	2.38e-3	5.92e-4	1.48e-4
order	-	2.02	2.01	2.00
$\ \mathbf{u} - \mathbf{u}_h\ _{\mathbf{L}^2(\Omega)}$	5.96e-4	7.24e-5	8.98e-6	1.12e-6
order	-	3.04	3.01	3.00
$\ p - p_h\ _{L^2(\Omega)}$	1.39e-3	1.56e-4	1.90e-5	2.36e-6
order	-	3.16	3.04	3.01

Polynomial degree $k' = 3$

h	1/8	1/16	1/32
$ \mathbf{u} - \mathbf{u}_h _{\mathbf{H}^1(\Omega)}$	5.39e-4	6.88e-5	8.76e-6
order	-	3.00	2.97
$\ \mathbf{u} - \mathbf{u}_h\ _{\mathbf{L}^2(\Omega)}$	3.42e-5	2.15e-6	1.36e-7
order	-	3.99	3.98
$\ p - p_h\ _{L^2(\Omega)}$	1.69e-4	9.44e-6	5.77e-7
order	-	4.16	4.03

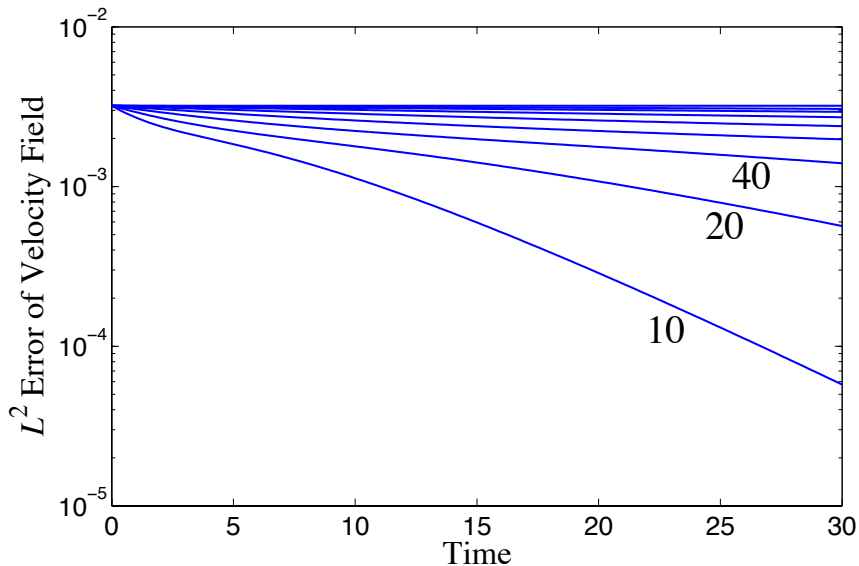


Figure 2: Two-dimensional Taylor-Green vortex flow: L^2 error of velocity field versus time at $Re = 10, 20, 40, 80, 160, 320, 640, 1280, \infty$ for a $k' = 1$ discretization with 16×16 elements. Time-step size chosen as $\Delta t = \min \left\{ h, \frac{h^2}{4\nu} \right\}$.

sufficiently small to ensure temporal discretization errors are of the same order as spatial discretization errors. It should be mentioned the use of the Crank-Nicolson method results in fully discrete schemes which automatically inherit the conservation structure of the corresponding semi-discrete schemes. The initial condition was chosen using \mathbf{L}^2 -projection into the discrete space of divergence-free velocity fields. Convergence rates obtained at time $t = 15$ for a flow of Reynold's number $Re = \frac{1}{\nu} = 100$ are provided in Table 1. Note from the \mathbf{L}^2 - the \mathbf{H}^1 -norms of the velocity error and the L^2 -norm of the pressure error optimally converge in h . To analyze the behavior of our method in time, we have plotted the \mathbf{L}^2 -norm of the velocity error versus time for a chosen spatial discretization and for a wide variety of Reynold's numbers in Figure 2. Note from the figure that our numerical error is bounded in time. Moreover, the numerical error decays roughly at the same rate as the exact solution. Indeed, we are able to reproduce a time-independed solution when $Re = \infty$. This indicates the nonlinear convection term has not interfered with the flow evolution of our discrete velocity solution.

To contrast our methodology with standard mixed flow discretizations, we repeated the above computations for a conservative Taylor-Hood finite element approximation. Again, the Crank-Nicolson method was employed to discretize in time. We found that the results obtained using this flow technology were unstable in general. To illustrate this, we have plotted in Figure 3 the \mathbf{L}^2 -norm of the velocity error versus time for a \mathbf{Q}_2/Q_1 Taylor-Hood discretization at $Re = \infty$ on a mesh with 8×8 elements. Note the exponential blow-up of the error in time. This blow-up is a direct result of unphysical energy growth stemming from the nonlinear convection term. Indeed, we have been unable to stably compute the discrete flow solution beyond a time

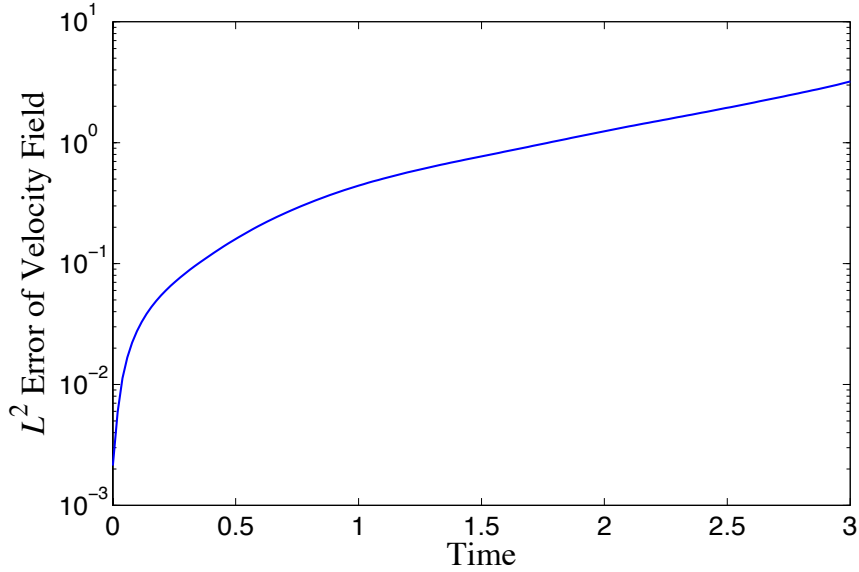


Figure 3: Two-dimensional Taylor-Green vortex flow: Blow-up of the L^2 velocity error for the conservative \mathbf{Q}_2/Q_1 Taylor-Hood discretization at $Re = \infty$ on a mesh with 8×8 elements. Time-step size chosen as $\Delta t = \frac{h}{40}$.

of $t = 5$. These results are a testament to the benefits of employing a conservative discretization which exactly preserves the divergence-free constraint.

8.2 Alternating Cylindrical Couette Flow

As a second numerical experiment, we consider the flow of a constant-property Newtonian fluid lying between a fixed inner cylinder and an oscillating outer cylinder. This flow scenario is referred to as alternating cylindrical Couette flow. The problem setup is illustrated in Figure 4. No external forcing is applied. The fluid is assumed to be at rest at time $t = 0$. Then, the outer cylinder begins to oscillate with angular velocity equal to $U_\theta = U \sin(\omega t)$, inducing the fluid to slip along with the outer cylinder. As time evolves, the flow field throughout the region between the two cylinders approaches a periodic (in time) steady state. The flow velocity associated with this steady state can be explicitly derived (see, for example, [49]) and is equivalent to

$$\mathbf{u} = \begin{bmatrix} u_\theta(r, t) \sin(\theta) \\ u_\theta(r, t) \cos(\theta) \end{bmatrix}$$

with

$$u_\theta(r, t) = U \text{Imag} \left(\frac{I_0(\gamma r) K_0(\gamma r_{in}) - I_0(\gamma r_{in}) K_0(\gamma r)}{I_0(\gamma r_{out}) K_0(\gamma r_{in}) - I_0(\gamma r_{in}) K_0(\gamma r_{out})} \exp \{i\omega t\} \right)$$

where (r, θ) are polar coordinates with respect to the center of the cylinders, $\gamma = \sqrt{i\omega\nu}$, and I_0 and K_0 are modified Bessel functions of the first and second kind,

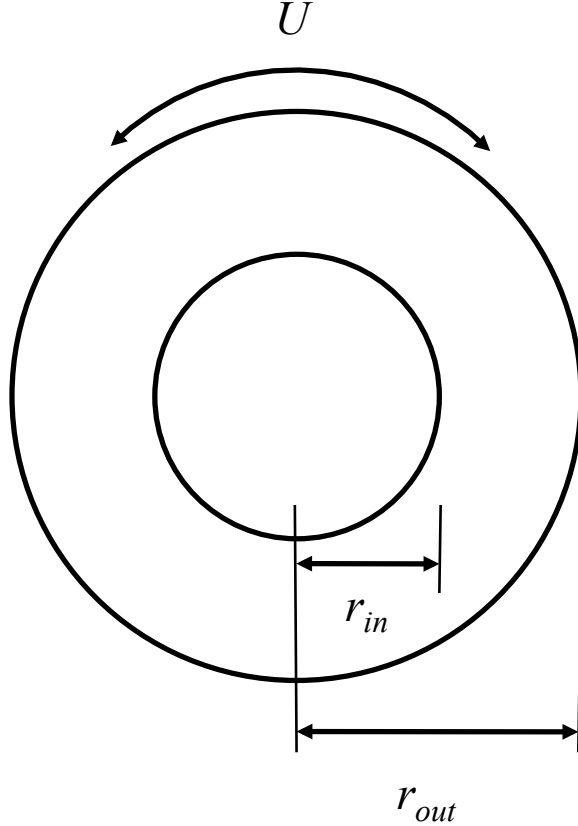


Figure 4: Alternating cylindrical Couette flow: Problem setup.

respectively. Unfortunately, no closed-form solution exists for the pressure field. The Reynold's number for this flow is taken to be

$$Re = \frac{2Ur_{in}}{\nu}.$$

In what follows, we assume $r_{in} = 1$, $r_{out} = 2$, and $U = 1$.

In Figure 5, we have plotted at time instances $t = 40.0, 40.2, 40.4, 40.6, 40.8, 41.0$ the exact angular velocity field associated with a $Re = 200$ flow subject to an oscillation frequency of $\omega = 5$. At these particular time instances, the flow has already reached the steady periodic state. Note from the figure that there is a small boundary layer attached to the outer cylinder. Further note that there is substantial flow reversal in a region away from the outer cylinder.

We believe alternating cylindrical Couette flow is an interesting and challenging numerical test problem for a number of reasons. First of all, the problem exhibits important symmetries that ideally should be preserved in a numerical simulation. As a consequence of these symmetries, the nonlinear advection term is exactly balanced by the pressure term. Second, the problem is characterized by strong shifts in angular momentum in time. Consequently, a methodology which admits angular momentum

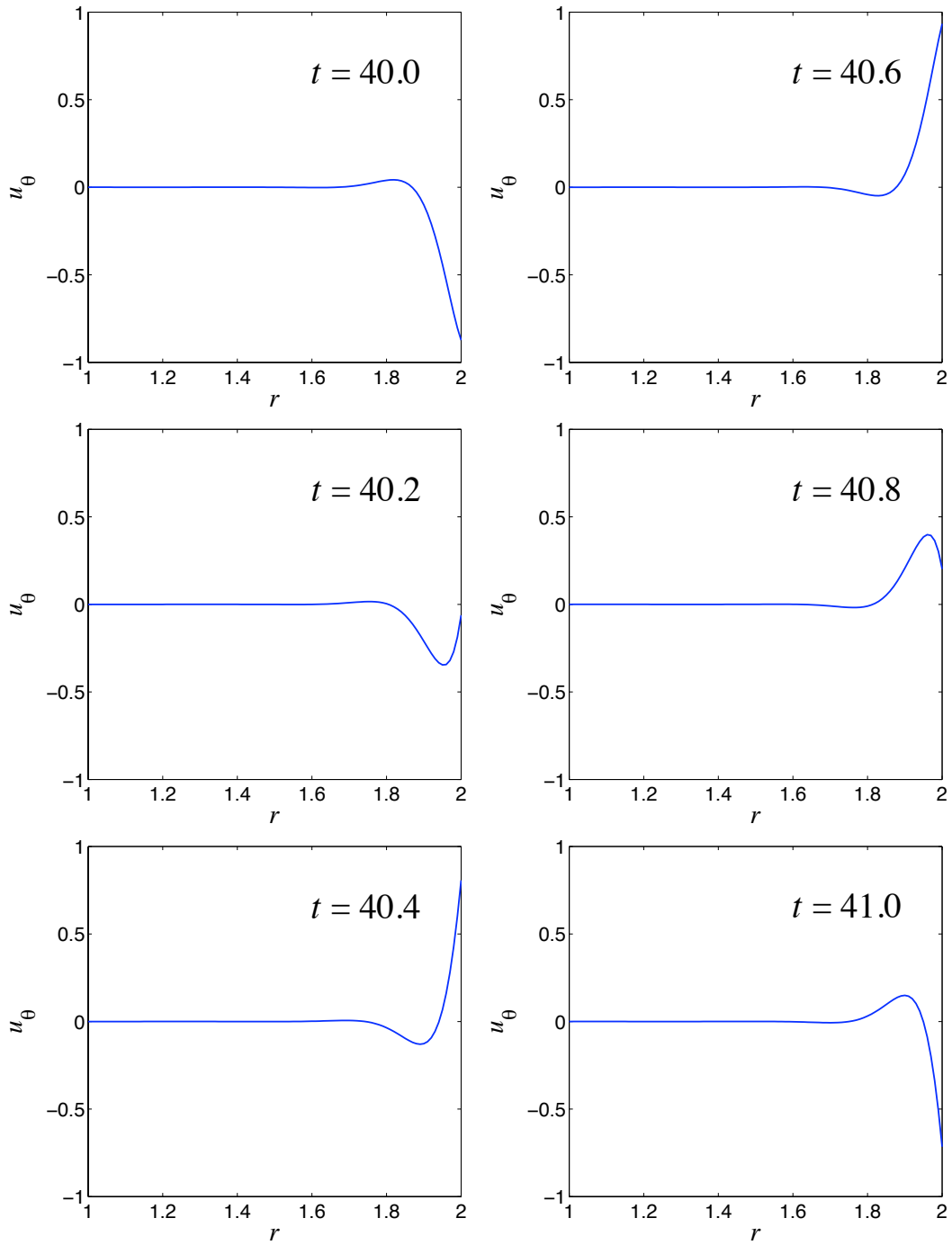


Figure 5: Alternating Couette flow: Plot of the angular velocity field at $Re = 200$ for $t = 40.0, 40.2, 40.4, 40.6, 40.8, 41.0$.

Table 2: Alternating cylindrical Couette flow: Convergence rates at $t = 40$ for $Re = 200$ and $\omega = 5$. Time-step size chosen as $\Delta t = h^{\frac{k'+1}{2}}$.

Polynomial degree $k' = 1$

h/h_0	1/8	1/16	1/32	1/64
$ \mathbf{u} - \mathbf{u}_h _{\mathbf{H}^1(\Omega)}$	2.99e0	1.79e0	1.05e0	5.51e-1
order	-	0.74	0.77	0.93
$\ \mathbf{u} - \mathbf{u}_h\ _{\mathbf{L}^2(\Omega)}$	9.35e-2	2.95e-2	8.86e-3	2.40e-3
order	-	1.66	1.74	1.88
$\ u_r - (u_r)_h\ _{L^2(\Omega)}$	0	0	0	0

Polynomial degree $k' = 2$

h/h_0	1/8	1/16	1/32	1/64
$ \mathbf{u} - \mathbf{u}_h _{\mathbf{H}^1(\Omega)}$	2.24e0	8.72e-1	2.14e-1	5.15e-2
order	-	1.36	2.03	2.06
$\ \mathbf{u} - \mathbf{u}_h\ _{\mathbf{L}^2(\Omega)}$	3.23e-2	7.00e-3	9.56e-4	1.26e-4
order	-	2.21	2.87	2.92
$\ u_r - (u_r)_h\ _{L^2(\Omega)}$	0	0	0	0

Polynomial degree $k' = 3$

h/h_0	1/8	1/16	1/32
$ \mathbf{u} - \mathbf{u}_h _{\mathbf{H}^1(\Omega)}$	1.51e0	1.84e-1	2.32e-1
order	-	3.04	2.99
$\ \mathbf{u} - \mathbf{u}_h\ _{\mathbf{L}^2(\Omega)}$	2.13e-2	1.27e-3	7.94e-5
order	-	4.07	4.00
$\ u_r - (u_r)_h\ _{L^2(\Omega)}$	0	0	0

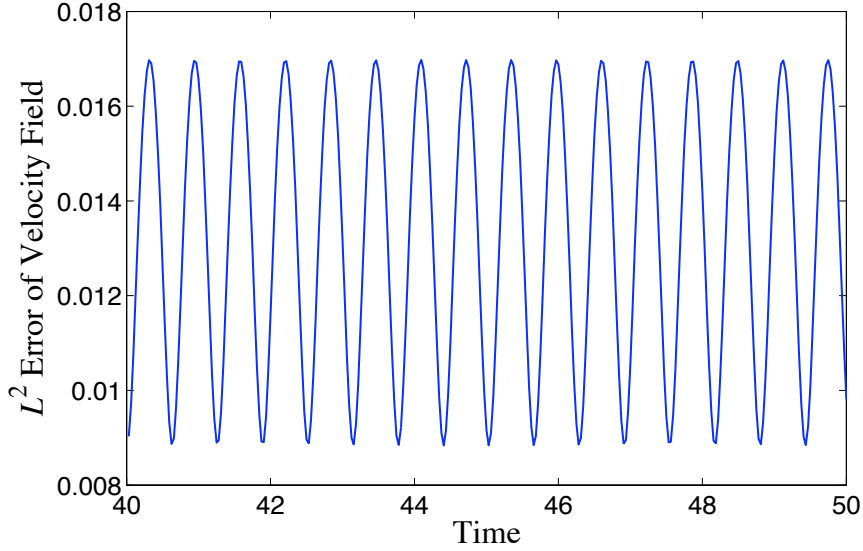


Figure 6: Alternating cylindrical Couette flow: L^2 error of velocity field versus time at $Re = 200$ for a $k' = 1$ discretization with 128×32 elements in the θ, r directions. The oscillation frequency for this simulation was chosen as $\omega = 5$, and the time-step size was chosen as $\Delta t = h$.

balance is preferred. Finally, the problem is characterized by the presence of boundary layers and flow reversal. Many flow technologies exhibit spurious oscillations when applied to problems harboring such features.

We have numerically simulated alternating cylindrical Couette flow using divergence-conforming B-spline discretizations of varying mesh size and polynomial degree. We utilized a polar mapping to represent the annular domain, and Nitsche’s method was invoked to enforce the slip condition along the cylinder surfaces. The resulting semi-discretizations satisfy an angular momentum balance law as discussed in Subsection 7.2. As in the last verification test, the Crank-Nicolson method was employed to discretize in time, and the time-step size was chosen to be

$$\Delta t = h^{\frac{k'+1}{2}},$$

sufficiently small to ensure temporal discretization errors are of the same order as spatial errors. Convergence rates obtained at $t = 40$ for a $Re = 200$ flow subject to an oscillation frequency of $\omega = 5$ are provided in Table 2. Note from the table that the \mathbf{L}^2 - and \mathbf{H}^1 -norms of the velocity error approach optimal convergence rates in h and that we have obtained axisymmetric velocity fields with zero radial component. To analyze the behavior of our method in time, we have plotted in Figure 6 the \mathbf{L}^2 -norm of the velocity error versus time for a chosen spatial discretization. Note from the figure that our numerical error is bounded and periodic in time. This indicates that our numerical solution, like the exact solution, has reached a periodic steady-state.

8.3 Three-Dimensional Taylor-Green Vortex Flow

As a third and final numerical experiment, we consider three-dimensional Taylor-Green vortex flow. Three-dimensional Taylor-Green vortex flow is one of the simplest systems in which one can study enstrophy production and the turbulence resulting from vortex stretching. The initial conditions for this flow are

$$\mathbf{u}_0(x, y, z) = \begin{bmatrix} \sin(x) \cos(y) \cos(z) \\ -\cos(x) \sin(y) \cos(z) \\ 0 \end{bmatrix}.$$

The flow is periodic in all three spatial directions in the domain $\Omega = (0, 2\pi)^3$ and exhibits a 64-fold symmetry which can be exploited in numerical simulation [9]. The Reynolds number for this flow is commonly taken to be

$$Re = \frac{1}{\nu}.$$

In Figure 7, we have reproduced time history plots of the dissipation rate

$$\epsilon = \frac{1}{|\Omega|} \int_{\Omega} 2\nu |\nabla^s \mathbf{u}|^2 d\mathbf{x} = \frac{1}{|\Omega|} \int_{\Omega} \nu |\nabla \mathbf{u}|^2 d\mathbf{x} = \frac{1}{|\Omega|} \int_{\Omega} \nu |\mathbf{curl} \mathbf{u}|^2 d\mathbf{x}$$

that were obtained by Brachet *et al.* in [9] via Fourier-based Direct Numerical Simulation (DNS) with 256^3 resolved modes. Note that the flow exhibits significant enstrophy production throughout the initial stages of flow evolution regardless of Reynold's number. At $Re = 100$, the time corresponding to the maximum dissipation rate is approximately $t \approx 4.75$. As the Reynolds number is increased, the time corresponding to the maximum dissipation rate gradually increases until it settles around a value of $t \approx 9$.

To simulate three-dimensional Taylor-Green vortex flow, we have utilized divergence-free B-spline discretizations of varying mesh size and polynomial degrees $k' = 1, 2, 3$. We have exploited symmetry conditions in order to solve the unsteady Navier-Stokes equations on the restricted domain $(0, \pi)^2$ and hence reduce the dimensionality of our discrete system by a factor of 8. A linear parametric mapping was utilized to describe the physical domain. The Crank-Nicolson method was employed to discretize viscous terms while the Adams-Bashforth multi-step method [2] was employed to discretize the nonlinear convective terms. This time discretization procedure allowed us to avoid the solution of a nonlinear algebraic problem at each time-step at the cost of losing some of the conservation structure of the semi-discrete method. A time-step size of $\Delta t = 0.05h$ was employed in all of our simulations. The initial condition was selected using \mathbf{L}^2 -projection into the discrete space of divergence-free velocity fields.

In Figure 8, we have depicted an enstrophy isosurface associated with the initial condition, and in Figure 9, we have depicted an enstrophy isosurface that was obtained at time $t = 6$ via a third-order B-spline simulation of $Re = 200$ flow on a spatial mesh comprised of 32×32 elements. This time roughly corresponds to the moment of maximum dissipation rate. Note from the figures that while the initial solution is

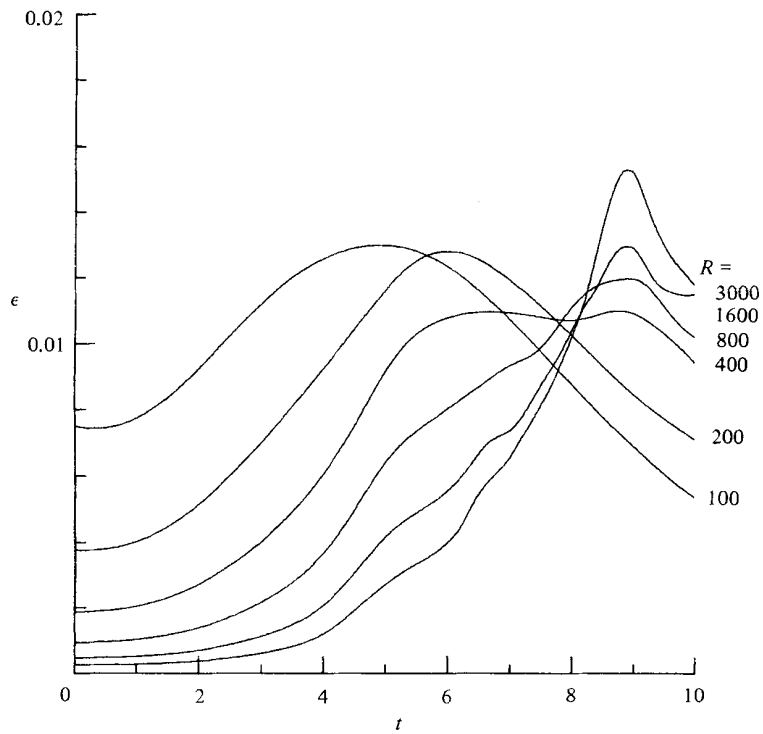
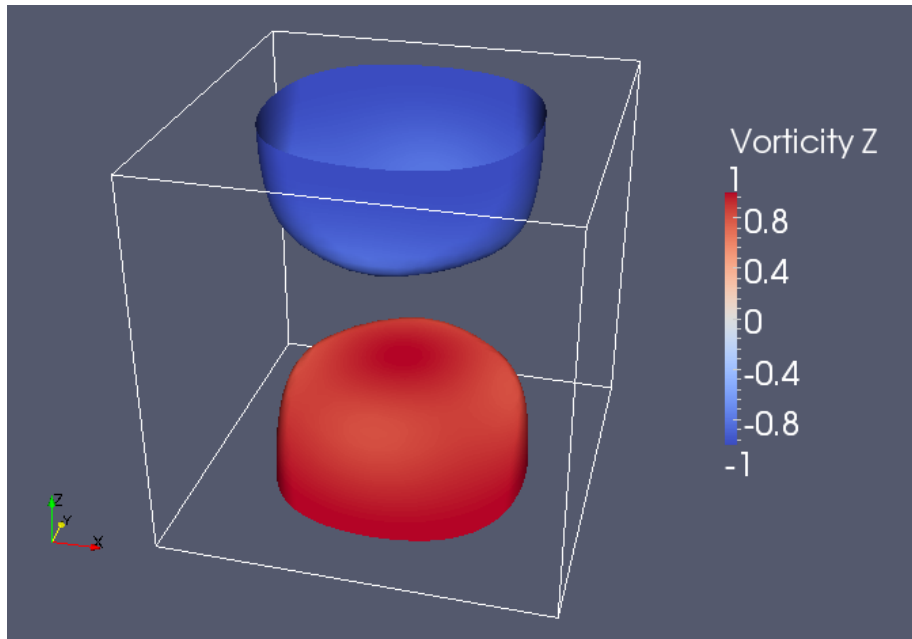
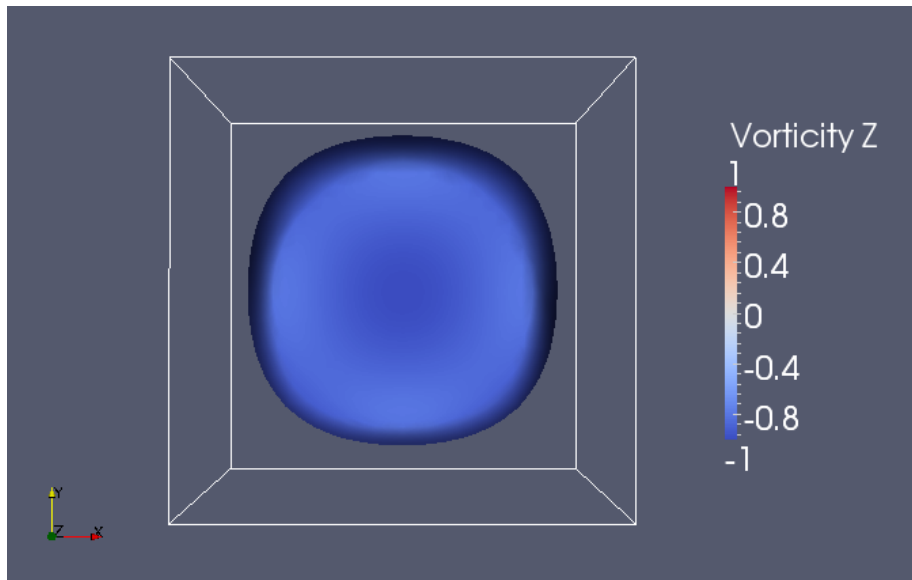


Figure 7: 3-D Taylor-Green vortex flow: Time history plots of the dissipation rate for various Reynold's numbers. Image reproduced from Brachet *et al.* [9] with permission from Cambridge University Press.

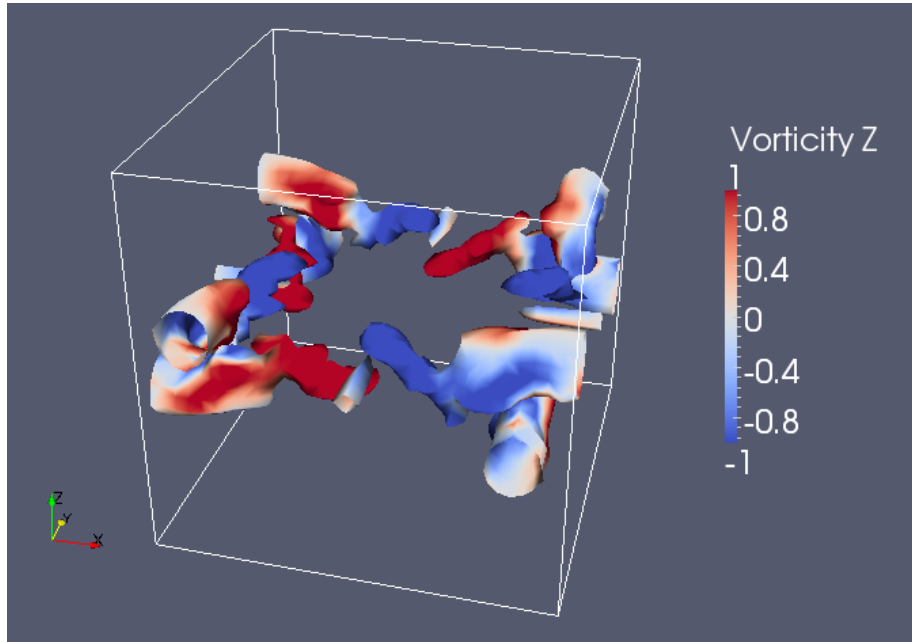


(a)

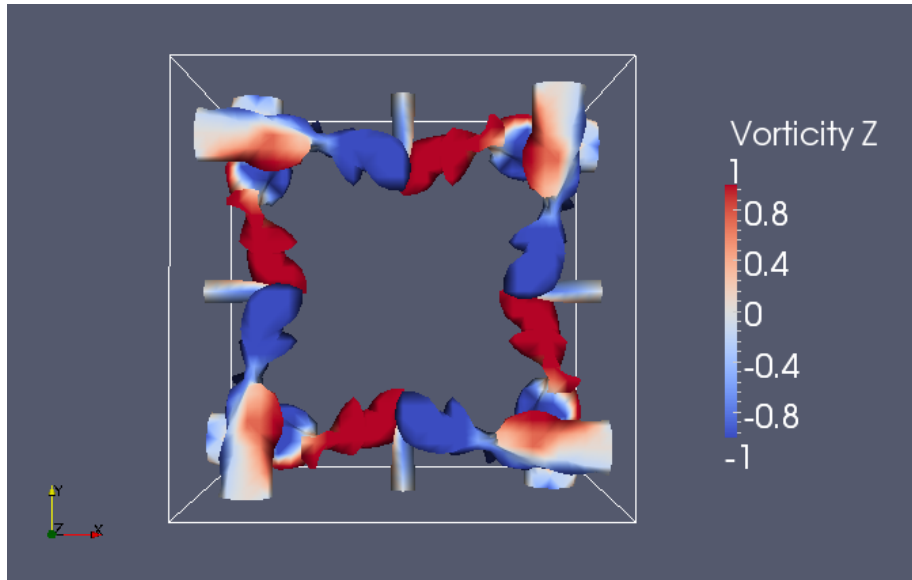


(b)

Figure 8: 3-D Taylor-Green vortex flow: Visualization of enstrophy isosurface colored by vertical vorticity at $t = 0$ for $Re = 200$. (a) 3-D View, (b) Overhead view. Visualization is restricted to the domain $(0, \pi)^3$.

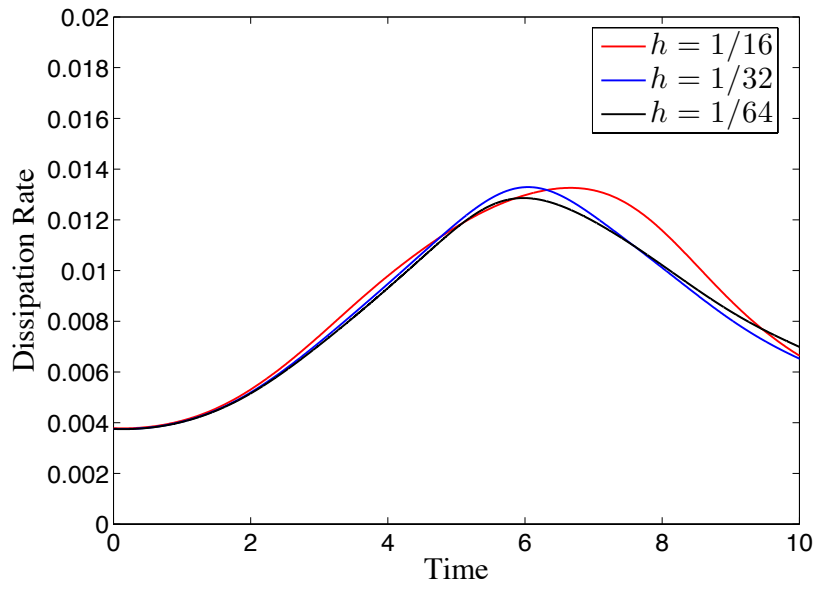


(a)

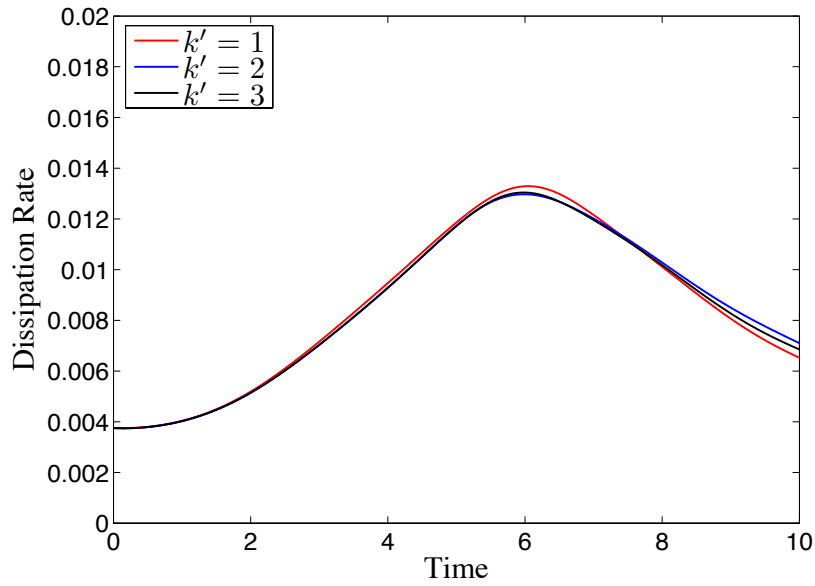


(b)

Figure 9: 3-D Taylor-Green vortex flow: Visualization of enstrophy isosurface colored by vertical vorticity at $t = 6$ for $Re = 200$. (a) 3-D View, (b) Overhead view. Visualization is restricted to the domain $(0, \pi)^3$.



(a)



(b)

Figure 10: 3-D Taylor-Green vortex flow: Convergence of dissipation rate time histories for $Re = 200$. (a) Convergence of $k' = 1$ discretizations under mesh refinement, (b) Convergence of $h = 1/32$ discretizations under degree elevation.

comprised of a single vortex on the restricted domain $(0, \pi)^3$, vortex stretching has separated the initial vortex into many vortical structures by time $t = 6$. Further note the vast amount of symmetry exhibited by the vortical structures. We found that this symmetry was preserved in all of our numerical experiments. In Figure 10(a), we have depicted the $Re = 200$ dissipation rate time histories associated with a sequence of refined $k' = 1$ discretizations. The dissipation rate time history on the finest mesh is virtually indistinguishable from the corresponding DNS time history depicted in Figure 7. The other dissipation rate time histories quickly converge in h . It should be noted that we have been able to stably compute arbitrary Reynold's number flow on the coarse mesh ($h = 1/16$), though the results were wildly inaccurate at long times due to a fine-scale pile-up of energy resulting from a lack of resolution. In Figure 10(b), we have depicted the $Re = 200$ dissipation rate time histories associated with $h = 1/32$ discretizations of varying polynomial degree. Note that the dissipation rate time histories quickly converge in k' . Furthermore, the $k' = 3$ dissipation rate time history nearly matches the corresponding DNS time history illustrated in Figure 7, though the $k' = 1, h = 1/64$ results are in slightly better agreement.

9 Conclusions

In this paper we have described the use of divergence-conforming B-spline discretizations for unsteady Navier-Stokes flows. These functions enable smooth, pointwise divergence-free solutions to be computed on geometrically mapped meshes. Consequently, conservation of mass is satisfied exactly, both globally and locally. Our semi-discrete variational equations are written in conservation form and thus preserve other important conservation and balance laws. This is in fact a consequence of the pointwise exactness of mass conservation. We note that heretofore no numerical method for the Navier-Stokes equations has been able to achieve similar attributes. Our focus in the work herein has been on Galerkin discretizations with weakly-enforced no-slip boundary conditions. To be more precise, we satisfy no-penetration boundary conditions strongly and the tangential boundary condition weakly. As we have documented in previous works, this treatment of the no-slip boundary condition is always *at least* as accurate as strong enforcement and, in the case of under-resolved boundary layer phenomena, often procedures remarkably accurate results. Furthermore, this approach provides a natural pathway to the computation of Euler flows as the kinematic viscosity takes on the limiting value of zero. In the computational setting, no changes to the degree-of-freedom structures need to be made when calculating Navier-Stokes and Euler flows, which proves very convenient.

The semi-discrete equations are shown to conserve linear and angular momentum, and discrete balance laws for vorticity, enstrophy, and helicity are also derived. The geometrical structure of solutions of the Navier-Stokes and Euler equations are intimately linked to the preservation of these conservation and balance laws. To illustrate the behavior of the methods on solutions in which geometrical structure is sensitive to the evolution of such quantities, we performed numerical calculations of two-dimensional Taylor-Green vortical flow, alternating cylindrical Couette

flow, and three-dimensional Taylor-Green vortical flow. In each case the structure-preserving behavior and quantitative accuracy are clearly evident, even on relatively coarse meshes. In addition to the computational verifications of the methodology, there are important theoretical implications: this is potentially the first instance of a structure-preserving methodology that might be used for DNS calculations on geometrically interesting domains. As such, it provides a numerical conduit for exploring fundamental flow physics on geometries never before explored.

This is a first but important step in a new area of computational fluid dynamics. To go further, much basic research needs to be pursued. To develop LES-level methods, stabilized and variational multiscale generalizations need to be developed, preserving the conservation/balance law structure, but extending it to arbitrarily high Reynolds numbers on mesh sizes that are approachable with contemporary computer hardware. In addition, the methods need to be made applicable to unstructured meshes with T-junctions (*i.e.*, “T-meshes”) and “extraordinary points”. We hope to play a significant role in these important pursuits.

Acknowledgements

John A. Evans and Thomas J.R. Hughes were partially supported by the Office of Naval Research under contract number N00014-08-0992. John A. Evans was additionally partially supported by the Department of Energy Computational Science Graduate Fellowship, provided under grant number DE-FG02-97ER25308. This support is gratefully acknowledged.

References

- [1] I Akkerman, Y Bazilevs, V M Calo, T J R Hughes, and S Hulshoff. The role of continuity in residual-based variational multiscale modeling of turbulence. *Computational Mechanics*, 41:371–378, 2008.
- [2] F Bashforth and J C Adams. *Theories of Capillary Action*. London: Cambridge University Press, 1883.
- [3] Y Bazilevs and I Akkerman. Large eddy simulation of turbulent Taylor-Couette flow using isogeometric analysis and residual-based variational multiscale method. *Journal of Computational Physics*, 229:3402–3414, 2010.
- [4] Y Bazilevs, V M Calo, J A Cottrell, T J R Hughes, A Reali, and G Scovazzi. Variational multiscale residual-based turbulence modeling for large eddy simulation of incompressible flows. *Computer Methods in Applied Mechanics and Engineering*, 197:173–201, 2007.
- [5] Y Bazilevs and T J R Hughes. Weak imposition of Dirichlet boundary conditions in fluid mechanics. *Computers and Fluids*, 36:12–26, 2007.

- [6] Y Bazilevs, C M Michler, V M Calo, and T J R Hughes. Weak Dirichlet boundary conditions for wall-bounded turbulent flows. *Computer Methods in Applied Mechanics and Engineering*, 196:4853–4862, 2007.
- [7] Y Bazilevs, C M Michler, V M Calo, and T J R Hughes. Isogeometric variational multiscale modeling of wall-bounded turbulent flows with weakly-enforced boundary conditions on unstretched meshes. *Computer Methods in Applied Mechanics and Engineering*, 199:780–790, 2010.
- [8] L C Berselli and D Cordoba. On the regularity of the solutions to the 3D Navier-Stokes equations: A remark on the role of helicity. *Comptes Rendus Mathematique*, 347:613–618, 2009.
- [9] M E Brachet. Small-scale structure of the Taylor-Green vortex. *Journal of Fluid Mechanics*, 130:411–452, 1983.
- [10] S C Brenner. Korn’s inequalities for piecewise H^1 vector fields. *Mathematics of Computation*, 73:1067–1087, 2003.
- [11] A Buffa, C de Falco, and G Sangalli. Isogeometric analysis: Stable elements for the 2D Stokes equation. *International Journal for Numerical Methods in Fluids*, 2010. To appear.
- [12] A Buffa, J Rivas, G Sangalli, and R Vázquez. Isogeometric discrete differential forms in three dimensions. *SIAM Journal on Numerical Analysis*, 49:818–844, 2011.
- [13] A Buffa, G Sangalli, and R Vázquez. Isogeometric analysis in electromagnetics: B-splines approximation. *Computer Methods in Applied Mechanics and Engineering*, 199:1143–1152, 2010.
- [14] L Caffarelli, R Kohn, and L Nirenberg. Partial regularity of suitable weak solutions of the Navier-Stokes equations. *Communications in Pure and Applied Mathematics*, 35:771–831, 1982.
- [15] J A Cottrell, T J R Hughes, and Y Bazilevs. *Isogeometric Analysis: Toward Integration of CAD and FEA*. Wiley, 2009.
- [16] J Crank and P Nicolson. A practical method for numerical evaluation of solutions of partial differential equations of the heat conduction type. *Mathematical Proceedings of the Cambridge Philosophical Society*, 43:50–67, 1947.
- [17] C R de Boor. *A Practical Guide to Splines*. Springer-Verlag, 1978.
- [18] C R Doering. The 3D Navier-Stokes Problem. *Annual Review of Fluid Mechanics*, 41:109–128, 2009.
- [19] J A Evans. *Divergence-free B-spline Discretizations for Viscous Incompressible Flows*. PhD thesis, The University of Texas at Austin, 2011.

- [20] J A Evans, Y Bazilevs, I Babuška, and T J R Hughes. n -widths, sup-infs, and optimality ratios for the k -version of the isogeometric finite element method. *Computer Methods in Applied Mechanics and Engineering*, 198:1726–1741, 2009.
- [21] J A Evans and T J R Hughes. Explicit trace inequalities for isogeometric analysis and parametric finite elements. Technical report, ICES Report 11-17, 2011.
- [22] J A Evans and T J R Hughes. Isogeometric divergence-conforming B-splines for the Darcy-Stokes-Brinkman equations. Technical report, ICES Report 12-03, 2012.
- [23] J A Evans and T J R Hughes. Isogeometric divergence-conforming B-splines for the steady Navier-Stokes equations. Technical report, ICES Report 12-15, 2012.
- [24] J-L Guermond. Faedo-Galerkin weak solutions of the Navier-Stokes equations with Dirichlet boundary conditions are suitable. *Journal de Mathematiques Pures et Appliquees*, 88:87–106, 2007.
- [25] J-L Guermond. On the use of the notion of suitable weak solutions in CFD. *International Journal for Numerical Methods in Fluids*, 57:1153–1170, 2008.
- [26] J G Heywood and R Rannacher. Finite element approximation of the non-stationary Navier-Stokes problem. I. Regularity of solutions and second-order error estimates for spatial discretization. *SIAM Journal on Numerical Analysis*, 19:275–311, 1982.
- [27] J G Heywood and R Rannacher. Finite element approximation of the nonstationary Navier-Stokes problem. II. Stability of solutions and error estimates uniform in time. *SIAM Journal on Numerical Analysis*, 23:750–777, 1986.
- [28] J G Heywood and R Rannacher. Finite element approximation of the nonstationary Navier-Stokes problem. III. Smoothing property and higher order error estimates for spatial discretization. *SIAM Journal on Numerical Analysis*, 25:489–512, 1988.
- [29] K Höllig. *Finite Element Methods with B-splines*. Society for Industrial and Applied Mathematics, 2003.
- [30] E Hopf. Über die Anfangswertaufgabe für die hydrodynamischen Grundgleichungen. *Mathematische Nachrichten*, 4:213–231, 1950/51.
- [31] T J R Hughes, G Engel, L Mazzei, and M G Larson. The continuous Galerkin method is locally conservative. *Journal of Computational Physics*, 163:467–488, 2000.
- [32] A A Kiselev and O A Ladyzhenskaya. On the existence and uniqueness of solutions of the non-stationary problems for flows of non-compressible fluids. *Izvestiya Rossiiskoi Akademii Nauk. Seriya Matematicheskaya*, 9:655–680, 1957.

- [33] A G Kravchenko, P Moin, and R Moser. Zonal embedded grids for numerical simulation of wall-bounded turbulent flows. *Journal of Computational Physics*, 127:412–423, 1996.
- [34] A G Kravchenko, P Moin, and R Moser. B-spline method and zonal grids for simulation of complex turbulent flows. *Journal of Computational Physics*, 151:757–789, 1999.
- [35] P D Lax and A N Milgram. Parabolic equations. In *Contributions to the Theory of Partial Differential Equations (AM-33)*, pages 167–190. Princeton University Press, 1974.
- [36] J Leray. Sur le mouvement d’un liquide visqueux emplissant l’espace. *Acta Mathematica*, 63:193–248, 1934.
- [37] P Loulou, R D Moser, N N Mansour, and B J Cantwell. Direct numerical simulation of incompressible pipe flow using a B-spline spectral method. Technical report, NASA-Ames Research Center, 1997.
- [38] H K Moffatt. Simple topological aspects of turbulent vorticity dynamics. In T Tatsumi, editor, *Turbulence and Chaotic Phenomena in Fluids*. Elsevier, 1984.
- [39] H K Moffatt. Fixed points of turbulent dynamical systems and suppression of nonlinearity. In J L Lumley, editor, *Whither Turbulence?*, pages 250–257. Springer-Verlag, 1990.
- [40] H K Moffatt. Spiral structures in turbulent flow. In *Proceedings of the IMA Conference “Wavelets, Fractals and Fourier Transforms”*, Cambridge, 1991.
- [41] H K Moffatt and A Tsoniber. Helicity in laminar and turbulent flow. *Annual Reviews of Fluid Mechanics*, 24:281–312, 1992.
- [42] J A Nitsche. Über ein Variationsprinzip zur Lösung von Dirichlet-Problemem bei Verwendung von Teilräumen, die keinen Randbedingungen unterworfen sind. *Abhandlungen aus dem Mathematischen Seminar der Universität Hamburg*, 36:9–15, 1971.
- [43] M Olshanskii and L G Rebholz. Note on helicity balance of the Galerkin method for the 3D Navier-Stokes equations. *Computer Methods in Applied Mechanics and Engineering*, 199:1032–1035, 2010.
- [44] P A Raviart and J M Thomas. A mixed finite element method for second order elliptic problems. *Lecture Notes in Mathematics*, 606:292–315, 1977.
- [45] V Scheffer. Hausdorff measure and the Navier-Stokes equations. *Communications in Mathematical Physics*, 55:97–112, 1977.
- [46] L L Schumaker. *Spline functions: Basic theory*. Cambridge Mathematical Library, Cambridge University Press, 2007.

- [47] D B Spalding. A single formula for the law of the wall. *Journal of Applied Mechanics*, 28:444–458, 1961.
- [48] H Triebel. *Interpolation Theory, Function Spaces, Differential Operators, Second Edition*. Johann Ambrosius Barth, 1995.
- [49] D Vieru, W Akhtar, C Fetecau, and C Fetecau. Starting solutions for the oscillating motion of a Maxwell fluid in cylindrical domains. *Meccanica*, 42:573–583, 2007.